White−light flares on cool stars in the *Kepler* Quarter 1 Data

Lucianne M. Walkowicz[1], Gibor Basri[1], Natalie Batalha[2], Ronald L. Gilliland[3], Jon Jenkins[2], William J. Borucki[2], David Koch[2], Doug Caldwell[2], Andrea K. Dupree[4], David W. Latham[4], Soeren Meibom[4], Steve Howell[5], Timothy M. Brown[6], Steve Bryson[2]

ABSTRACT

We present the results of a search for white light flares on the ∼23,000 cool dwarfs in the *Kepler* Quarter 1 long cadence data. We have identified 373 flaring stars, some of which flare multiple times during the observation period. We calculate relative flare energies, flare rates and durations, and compare these with the quiescent photometric variability of our sample. We find that M dwarfs tend to flare more frequently but for shorter durations than K dwarfs, and that they emit more energy relative to their quiescent luminosity in a given flare than K dwarfs. Stars that are more photometrically variable in quiescence tend to emit relatively more energy during flares, but variability is only weakly correlated with flare frequency. We estimate distances for our sample of flare stars and find that the flaring fraction agrees well with other observations of flare statistics for stars within 300 pc above the Galactic Plane. These observations provide a more rounded view of stellar flares by sampling stars that have not been pre-selected by their activity, and are informative for understanding the influence of these flares on planetary habitability.

Subject headings: stars: low mass — stars: magnetic activity — stars: emission lines — stars: flares

[1]Astronomy Department, University of California at Berkeley, 601 Campbell Hall, Berkeley, CA 94720

[2]NASA Ames Research Center, Moffett Field, CA 94035

[3]Space Telescope Science Institute, Baltimore, MD 21218

[4]Harvard-Smithsonian Center for Astrophysics, Cambridge, MA 02138

[5]National Optical Astronomy Observatory, Tucson, AZ 85719

[6]Las Cumbres Observatory Global Telescope, Goleta, CA 93117

1. Introduction

Flares are short-lived but intense releases of energy, caused by the reconnection of loops of magnetic field in the outer atmospheres of active stars. During these reconnection events, the field geometry reconfigures to a lower energy state, often accelerating energetic particles down towards the stellar atmosphere and causing a plethora of observable effects over a wide range in wavelength (for a recent review of flare processes, see Benz & Güdel 2010). On the Sun, our ability to spatially resolve the surface allows flares to be observed in rich detail with high cadence, and so much of our understanding of flare processes and their consequences comes from observations of solar flares. Unfortunately, the luxury of spatial resolution is not available for flares on stars other than our Sun, and so stellar flare studies rely instead on time−resolved photometry or spectroscopy.

Stellar flares long ago revealed themselves to be somewhat different from the standard solar model. Stars cooler than our Sun, such as the K and M dwarfs, have flares that seem both surprisingly energetic (flares on active M dwarfs are typically $10 - 1000$ times as energetic as solar flares) and qualitatively different than solar flares, showing strong continuum or "white light" emission, which resembles a 9000−10,000K blackbody superimposed over the quiet spectrum of the star (Haisch et al. 1991; Hawley & Pettersen 1991). White light emission in solar flares is usually concentrated in small areas near the footpoints of emerging magnetic field lines, is spatially associated with hard X−ray emission, and does not appreciably affect the integrated optical brightness of the Sun (e.g. Watanabe et al. 2010). By contrast, dramatic brightening due to white light emission is the photometric hallmark of cool star flares. The white light emission in these flares has been inferred to cover a much larger fraction of the visible stellar surface than the white light emission seen in solar flares– for example, the recently reported white light flare emission on the M dwarf YZ CMi was inferred to cover 0.22% of the visible disc (Kowalski et al. 2010), or roughly $\sim$400 Mm^2, while the 2002 solar flare discussed in Potts et al. (2010) had a $\sim$20 Mm^2 emitting area. These observed differences likely have to do with the changing topology of the magnetic field as one moves to cooler stars. Active stars near the convective boundary ($M_\star < 0.4 M_\odot$) tend to have large scale, non-axisymmetric fields and larger areal coverage of active regions (Saar & Linsky 1985; Johns-Krull & Valenti 1996; Donati et al. 2008; Reiners & Basri 2009). Although stellar flares are fundamentally multiwavelength phenomena and have been observed across the electromagnetic spectrum (e.g. Hawley et al. 2003; Osten et al. 2005; Hawley et al. 2007) photometric flare campaigns in the optical tend to focus on observations in the blue due to the higher contrast of the flare white light emission with the photosphere (and thus enhanced detectability of the flare).

Open questions regarding the overall rate and properties of flares have recently come to

the forefront, due to the effects of flares on planetary habitability and as a source of Galactic transients in new time domain surveys (Segura et al. 2010; Tyson 2006). Typically, stellar flare research has focused on detailed studies of a few of the most active known stars, largely due to the reluctance of astronomers and time allocation committees to spend telescope time observing a star which may not do anything in the course of a night. These studies have concentrated in particular on the most active M dwarfs, the dMe stars– so dubbed due to their powerful Hα (e)mission lines, indicative of strong magnetic activity. The seminal work of Lacy et al. (1976) determined the rates and energy distributions of flares for 8 active M dwarfs, and has long been the most detailed optical study of flare rates to date. However, little is known about how often flares occur on stars with moderate activity. Cool stars with Hα *absorption* are often also chromospherically active, albeit at a lower level, and have also been serendipitously observed to flare amongst stars *not* pre-selected for their activity (Walkowicz et al. 2008; Kowalski et al. 2009). In both the Sun and dMe stars, the probability distributions of flare energies are best described by a power law, indicating that small flares are more common than large (Charbonneau et al. 2001; Shakhovskaia 1989; Lu & Hamilton 1991). Much work has been done on the Sun to quantify the index that sets the slope of this power law, as the proportion of small flares to large determines whether so-called "nanoflares" are capable of being a significant source of coronal heating. However, dMe stars are quite different from the Sun, and it is not yet known whether the distribution of flare energies can be described by a power law for stars of all spectral types, and whether the indices of these power laws are the same (indicating a common physical process).

In this paper, we investigate flares found from observations of stars by the *Kepler* mission (Koch et al. 2010). While *Kepler*'s primary objective is the detection of exoplanets, its constant monitoring of thousands of cool stars allows us to probe flares in a sample unlike any targeted for flare searches before. *Kepler* provides unmatched precision photometry, but does so only in a broad bandpass filter (400 − 900 nm). The contrast between the flare emission and the quiescent stellar photosphere is therefore lower than for observations performed in a blue filter, and the lack of color information makes it difficult to use previously defined metrics such as flare color indices (Kowalski et al. 2009). We therefore searched for the most obvious deviations from quiescence, likely to be astrophysical in nature rather than instrumental, and report our first results from a search for white light flares in the *Kepler* Quarter 1 observations here. In the next section, we outline the sample selection and the flare search algorithm, as well as how each flare was measured, including a new definition for a useful metric we use here. In the last section, we discuss the implications of our results and potential areas of future research.

2. Data Selection and Analysis

The *Kepler* Quarter 1 long cadence data consist of 33.5 days of photometry sampled every 30 minutes, taken between 13 May 2009 and June 15 2009. In this paper, we work from the raw simple aperture photometry provided in the publicly released Quarter 1 FITS files, under the AP_RAW_FLUX keyword. The "raw" photometry is not truly raw: it has been corrected for the background, flat fielded, subjected to cosmic ray removal and aperture summed. The resulting photometry still contains some instrumental effects and artifacts, most notably long term trends over the quarter due to differential velocity aberration (Caldwell et al. 2010; Jenkins et al. 2010) We remove these trends and instrumental effects with our own analysis pipeline, described in detail in Basri et al. (2010b). In brief, our treatment of the data removes likely instrumental trends but leaves shorter-term spot-like variability intact. While some of the long term trends we remove over Q1 may be astrophysical in nature, we err on the side of caution as we cannot distinguish between true and instrumental trends over only a single month of data. For the purposes of searching for transient events like flares, long trends in the data are immaterial, as they occur over a much longer timescale (i.e. weeks) than the relatively brief duration of flares (i.e. hours).

2.1. Sample Selection

Our flare search sample consists of all stars that are classified in the *Kepler* Input Catalogue (KIC; Latham et al. 2005) as having logg ≥ 4.2 and $T_{eff} \leq 5150$ K, corresponding to 23,253 main sequence stars later than K0V[7]. The entire sample is detailed in Table 1, which is available in its entirety in the electronic version of this paper. Candidate flare events were initially identified by an automated search of all cool dwarf lightcurves meeting the KIC criteria outlined above. Our search algorithm has three adjustable parameters, the threshold, smoothing, and width. The threshold is the multiple of the standard deviation, excluding points that are extreme outliers from the norm, above which a point is flagged as a significant brightness change. The smoothing is the number of points over which to median filter the lightcurve to minimize point-to-point variations– the smoothed lightcurve is ultimately subtracted from the raw lightcurve, which removes most of the quiescent stellar variability and allows shorter timescale events to be found more easily. Lastly, the width is the minimum number of contiguous points that must lie above the threshold before an event will be flagged as a potential flare. The appropriate values for these search parameters were

[7]Our sample includes all exoplanetary search targets that are classified in the KIC, but excludes targets assigned to *Kepler* GO observers.

developed by experimentation between the automatic flare finder and a by-eye flare search on a test set of stars, the M dwarfs. A subset of the ∼2300 M dwarf lightcurves was first searched by eye for all outliers that appeared to be flares. These same lightcurves were then searched automatically using different values for the threshold, smoothing and width until the search algorithm was capable of finding the same set of flaring stars as the human eye. Naturally these two sets were not exactly the same, as the automatic search more easily found small, marginal candidate events than the human eye was capable of finding. We did ascertain that anything that was obviously a flare to the eye (possessing a clear impulsive rise and exponential decay) was found by the automatic flare finder. Ultimately we chose to smooth the lightcurves over a 10 hour interval, and events were flagged as candidate flares when a minimum of three contiguous points were found above a threshold of 4.5 times the standard deviation. As the *Kepler* lightcurves are sampled every 30 minutes, requiring a minimum number of points biases our search towards flares with a duration of 1.5 hours or longer, but this requirement also helps to distinguish astrophysical events from instrumental artifacts.

A search with the above parameters yielded 5784 candidate events, which were then vetted by eye and culled further to 2741 possible candidate flare stars. These 2741 candidate flare stars were again vetted by eye, and 373 stars were identified as having obvious flares showing the classical impulsive rise / exponential decay lightcurve shape. An additional 565 stars were identified as marginal cases, having potential-but-not-certain flares. In this paper, we focus our analysis on the 373 certain flare stars identified. We intend to revisit smaller events in the future, preferably when pixel-level data is available to rule out particle hits and other detector effects.

2.2. Measurement of Flares

The *Kepler* long cadence data is formed on board the spacecraft by summing 270 6-second integrations into successive blocks of 29.42 minutes. As such it is not *ideally* suited to the study of flares, as most flares evolve on timescales faster than the ∼30 minute cadence is capable of resolving. The peak of each flare is integrated into one cadence or another, but has somewhat lower contrast than if the cadence were shorter. For each lightcurve with flares, we masked out points tagged as flares and median filtered the remaining lightcurve to create a lightcurve with quiescent variability but no flares. We then subtract this quiescent lightcurve to remove slower modulation due to the presence of spots on the quiescent star. We then subtract off this fit, run the flare finder again to flag contiguous points that deviate above our threshold, and integrate the points that are tagged as part of the flare. What

results is essentially a photometric equivalent width for the flare, or

$$EW_{phot} = \int \frac{F_f - F_q}{F_q} dt$$

where F_f and F_q denote the flaring and quiescent flux, respectively. By analogy to equivalent width this quantity has the units of time, but can be intuitively thought of as the time interval over which the quiescent star emits as much energy as was released during the duration of the flare. EW_{phot} is a differential quantity, independent of distance and measured relative to the quiescent star.

We also calculate the duration of each flare, record the value of the brightest point in the flare, and if multiple flares occur on a single lightcurve, the time between each flare. In the interest of working with the data as is, we chose not to integrate assuming a typical flare lightcurve peak+exponential decay shape, nor do we perform detailed modeling of individual flares in this work. These studies are better suited to short cadence data (which was unavailable for the stars identified in this paper) and will be visited in future complementary work.

3. Results

The *Kepler* data offers a truly remarkable opportunity both to capture flares and to observe the quiescent variability of the star. Figure 1 shows four examples of flares found on M and K dwarfs, respectively, with the KIC effective temperatures shown at the top of each panel. In Figure 2, we show two of these lightcurves in further detail: the top panel shows the data as black points with flare points marked in red, and the fit to the star's quiescent variability is overplotted as a thick red line. Below, subpanels show examples of flares at an expanded scale, with the quiescent stellar flux removed− red diamonds indicate the points flagged as belonging to the flare event.

Table 2 presents the resulting number of flares for each star, the median EW_{phot}, flare peak brightness, duration, time between flares, the flare frequency, and percentage of time spent flaring (this table is available in its entirety in the electronic version of the paper).

In the top panel of Figure 3, we show the histogram of the effective temperature distribution of the entire cool dwarf sample, while the T_{eff} distribution for the sample of flaring stars appears in the lower, larger panel. Clearly, the number of stars on which flares were found increases with decreasing effective temperature, caused (at least in part) by the increasingly high contrast of white light flares for cooler stars.

In order to better quantify the effect of the flare-to-photosphere contrast on our flare detections, we added a 10,000K blackbody curve at varying areal coverage (so-called "fill factor") to a series of cool stellar template spectra (Pickles 1998) and convolved these synthetic flare spectra with the *Kepler* filter response. We then computed the instantaneous change in brightness (ΔF/F) we would expect to find for each spectral type for different fill factors. In Figure 4, we show effective temperature versus the peak ΔF/F in each flare, overplotted with lines of constant fill factor for a 10,000K blackbody.

Figure 4 shows a somewhat flat distribution of flare brightness enhancement over the range of T_{eff} in our sample. The relative dearth of very small flares with increasing effective temperature represents the detection threshold imposed by contrast effects− white light flares have a lower contrast on warmer stars, therefore small flares are more likely to go undetected. As effective temperature decreases, we are able to detect more small flares. There are fewer large flares detected towards cooler stars, which might be expected if the K dwarfs behave similarly to observed trends on M dwarfs: SDSS Stripe 82 observations of flaring M dwarfs show that higher mass cool stars tend to have more luminous flares than their cooler, less massive counterparts (Kowalski et al. 2010b). While at first glance the absolute value of the flux enhancements might seem quite small, we remind the reader that the relatively broad *Kepler* bandpass effectively "washes out" the effect of the flare on the photometry− for reference, aforementioned megaflare on YZ CMi, a cool M4.5V star, was 6 magnitudes in U, but only a 0.22% fill factor (Kowalski et al. 2010).

The detectability of a flare is a function not only of the relative contrast of the white light emission against the photosphere, but also the relative height of the flare against the intrinsic noise in the quiescent lightcurve, which is a function of magnitude. Candidate flares are required to have three consecutive points above our threshold as described in the previous section. Figure 5 shows the flare peak heights as a function of Kepler magnitude, with our detection threshold overplotted. As three red filled circles, we show where K0, K5 and M0 dwarfs would intersect this threshold if they were placed at a distance of 200 pc. At a given distance, intrinsically more luminous stars are brighter and therefore less noisy– therefore, although the emission from flares on these stars has lower contrast with their photospheres, one can actually detect smaller flares on them compared with cooler stars *at a given distance* because of their relatively lower noise.

Assuming that flares are associated with the same magnetic field formations that produce starspots, one might also expect there to be a correlation between the photometric variability of the lightcurve due to spots and the presence of flares. We quantify the bulk variability as "variability range", the range between the 5th and 95th percentile amplitude in the lightcurve (discussed in further detail in Basri et al. 2010b). In the center panel

of Figure 6, we show the relationship between the median EW_{phot} for the K dwarfs (black asterisks) and M dwarfs (red diamonds) and the photometric range in millimagnitudes. The flanking panels show the histograms of the range (at top) and EW_{phot} (at right) for the K and M dwarfs (solid black and red dashed lines, respectively). As flares were measured with the bulk photometric variability removed from the lightcurve, the trend between range and EW_{phot} indicates that flares with larger relative energy (as measured by EW_{phot}) do take place on stars with greater quiescent variability. The larger photometric variability is likely caused by larger spot coverage− this may in turn indicate either that spottier stars have intrinsically more energy released in a single flare, or perhaps that a greater number of spots implies a greater number of magnetic loops on the stellar surface, increasing the likelihood that multiple loops will be affected by a reconnection event (as in the case of flaring arcades on the Sun). It is notable that the distribution of ranges in our flare sample is fairly typical of other spot−modulated stars in the *Kepler* data (e.g. Basri et al. 2010a)− these stars do not represent a particularly variable sample amongst the rest of the stars in the Quarter 1 observations. Indeed, three stars in the flare sample did not have obvious spot modulation in quiescence. Due to the 30 day duration of Q1 we cannot discern rotation periods of longer than 30 days in the data, so it is possible that these flares are on stars with longer periods that are not evident in Q1 (as opposed to stars that are intrinsically flat in quiescence). We will revisit these stars in future quarters.

The duration and frequency of flares is particularly important to understand, both in the context of understanding the effect of flares on planetary habitability, and as a way of estimating Galactic transient rates in time domain surveys. In Figure 7, we show the median duration of all flares on each star versus EW_{phot} for all stars in the main panel, and as histograms of the duration in hours and the photometric equivalent width (at the top and right, respectively) for the K dwarfs (black solid line) and M dwarfs (red dashed line). EW_{phot} increases with the duration of the flares, which is to be expected as EW_{phot} is a time−integrated quantity. Interestingly, although the K dwarfs have more flares with durations of more than 4 hours than the M dwarfs, the photometric equivalent widths of the M dwarfs are slightly higher than the those of the K dwarfs. In other words, the M dwarf flares tend to release more energy relative to their quiescent flux in a given amount of time during a flare.

We also calculated the flare rates for our sample (defined as the number of flares detected divided by the time interval of the observation, 33.5 days), and the percentage of time spent flaring (defined as the total duration of all flares over the observing time, again 33.5 days). Figure 8 shows histograms of the percentage time spent flaring for flares of three bins in duration: 5 to 6 hours' duration (crosshatch filled), 4 to 5 hours' duration (diagonal line filled) and less than 4 hours duration (unfilled). It is evident that stars with longer median

duration flares actually spend a lower amount of the overall observation time flaring. In part, this behavior supports previous observations of individual stars where smaller flares were found to be more common than large flares (e.g. Lacy et al. 1976), but it also indicates that some stars may release the majority of their flare energy all at once in large events, while others undergo more frequent, smaller events. We investigated the magnitude distribution of the stars in each bin to ensure that long duration flares weren't preferentially being detected on brighter stars, and found that the observed effect is not a result of magnitude (and thus detection) bias.

In the lower panel of Figure 9, we show flare rate as a function of effective temperature. The top panel of this figure shows two normalized histograms, one for the K dwarfs (solid black line) and one for the M dwarfs (dashed red line). While the two samples have comparable relative populations of stars with low flare frequency ($0.1 - 0.2$ hr^{-1}), proportionally more M dwarfs make up the most frequently flaring stars, while the K dwarfs dominate the population who flare least frequently. M dwarfs therefore flare more often than K dwarfs, but for shorter durations, and during flares release more energy relative to their quiescent flux in a given time than their more mssive cousins.

In Figure 10, we show that while there is a loose correlation between the photometric range of our sample and the flare frequency, overall stars of different flare frequency are found over a large spread in range. One might expect that larger photometric variability (presumably due to larger spot coverage) might lead to more frequent flaring−the greater the number of spots, the greater the number of magnetic loops protruding from the stellar surface, and therefore the more potential sites for flares to take place. The fact that this is only a weak correlation implies that the relationship between having a great number of magnetic structures and the frequency of flares is not strictly causal− if a flare event in one active region played some role in "triggering" flares in neighboring regions, one would likely see a more direct correlation between the range and the flare frequency.

Lastly, we examined the spatial distribution of the flare sample, as it has been noted that cool stars with a greater |Z| distance from the Galactic plane flare less frequently than stars in the solar neighborhood (West et al. 2008). This observed drop−off in flare rate is due to the fact that older, less active stars have had a longer time in which to undergo dynamical interactions, thus scattering them further out of the plane. As *Kepler* observes in only one field (100 deg^2 centered on 19h 22m 40s, $+44^{\rm deg}$ $30'$ $00''$), an estimate of the |Z| distance is relatively simple trigonometry. We take the Sun to be 15 pc above the plane (Cohen 1995, Binney et al. 1997, Ng et al. 1997). All the stars in our flare sample have SDSS and 2MASS colors, for which there are existing photometric parallax relations (Bochanski et al. 2010; Covey et al. 2007). The left panel of Figure 11 shows the distribution of the flaring fraction

for the entire sample as a function of distance; clearly stars in the local neighborhood make up the majority of the flare sample. The right panel of this same figure shows the flare fraction by spectral type (K dwarfs: solid black line, M dwarfs: dashed red line)− the local flare fraction is heavily dominated by the M dwarfs. This result fits nicely with previous studies of active M dwarfs, e.g. Hawley et al. (1996), who found that up to ∼60% of M dwarfs in the solar neighborhood had Hα in emission.

4. Conclusions and Future Work

The *Kepler* data provide a new view of white light stellar flares, sampling a population of stars of varying activity rarely included in traditional flare studies. *Kepler*'s unprecedented photometric precision also provides simultaneous information on the quiescent variability of these flare stars. In this work, we have defined a new flare measure, the photometric equivalent width (EW_{phot}), which expresses the flare energy relative to the quiescent luminosity of the star. We conducted an automated search for flares amongst the cool dwarfs (classified in the *Kepler* Input Catalog as $T_{eff} \leq 5150$ K and logg ≥ 4.2) during the 33.5 days of *Kepler*'s Quarter 1 observations. We vetted the candidate events by eye, and found 373 stars which possessed one or more obvious white light flares.

In comparing the photometric variability of the quiescent lightcurves (as quantified by our "variability range" statistic), we observe that stars with larger quiescent variability (and thus larger spot coverage) seem to have intrinsically larger flares relative to their quiescent energy output (i.e. larger EW_{phot}). We also find that the distribution of observed flare peaks as a function of effective temperature is somewhat flat−− in part this trend is caused by the difficulty in detecting smaller flares on the warmer K dwarfs, as the contrast between the white light flare emission and the stellar photosphere is less than for cooler stars. However, we find fewer flares with large peaks on the M dwarfs versus the K dwarfs, while the M dwarfs tend to have somewhat larger EW_{phot} and shorter duration flares than the K dwarfs. Taking these observations together, we infer that M dwarf flares evolve faster than K dwarf flares, such that their flaring energy output relative to their quiescent luminosity is higher than that of the K dwarfs.

The time domain behavior of our flare sample is also quite interesting− in examining the frequency of flares, binned by the median duration of flares on each star, we find that longer duration flares tend to happen on stars that flare less frequently. Some stars may therefore release the majority of their flare energy in less frequent long duration events, while others release relatively less energy in a single event but flare more often. This trend appears to be a function of spectral type: overall, the M dwarfs make up the most frequently flaring

stars in our sample, flaring more often (but for shorter durations) than K dwarfs, and release more energy relative to their quiescent flux in a given time than their more massive K dwarf cousins. While a single month of data is too short to properly comment on the probability distribution of flares, the ongoing monitoring of these flare stars with *Kepler* will allow us to delve into that question in the near future.

Our flare sample is distributed over a few hundred parsecs above the Galactic plane, allowing us to calculate the flare fraction of our stars as a function of |Z|. In agreement with previous studies of M dwarf flare activity, we find that the flaring fraction of M dwarfs reaches roughly 50% in the local neighborhood. The K dwarfs have a far lower flare fraction, under 10% even locally, but as there are so many more K dwarfs in our sample, their population effectively dilutes the flare fraction when the sample is taken as a whole, such that only ∼10% of nearby stars flare.

This work provides important clues to the ongoing question of how stellar flares affect planetary habitability. The frequency of flares is a crucial piece of information because after a flare impacts and modifies the photochemistry of the planetary atmosphere, the atmosphere takes some time to return to its preflare state. If flares recur on shorter timescales than the atmospheric re−equilibration time, it is possible that the buildup of photochemical flare by−products will permanently alter the planet's atmosphere (e.g. Segura et al. 2010). To the many open questions regarding planetary habitability, we add one more: in the establishment or maintenance of a hospitable planet, is it preferable to be affected by longer duration, less frequent flares, or shorter, more frequent and more energetic flares? This question is most relevant during the youth of the star-planet system– activity in cool stars, M dwarfs in particular, declines strongly with age (West et al. 2008). The distribution in |Z| of our sample indicates that we are preferentially studying a young thin disk population, which flares relatively frequently– the majority of these stars' exceedingly long main sequence lifetimes are spent in relative quietude.

In future work, we intend to compare the rate and relative energy of flares with stellar rotation period, using the rotation analysis discussed in Basri et al. (2010b). Additional quarters of *Kepler* data will provide longer duration lightcurves, permitting us to associate flare properties with rotation rate and differential rotation.

We would also like to revisit smaller flares in the sample. The *Kepler* pixel-level data (the actual pixels in each aperture, rather than their summed total) will eventually become available for these stars. These data can be used to ascertain the astrophysical nature of relatively small brightness changes by seeing whether the change in brightness is associated with the target star or is caused by a brightness fluctuation on a neighboring pixel. We also intend to address the white light flare occurrence on solar type stars− although the contrast

of the white light emission against a roughly solar temperature photosphere is expected to be quite small, *Kepler*'s precision offers the best chance of detecting such events. While the white light emission on the Sun is small and quite localized, it is as yet unknown whether that is a trait of solar type stars in general, or just one solar type star in particular.

LMW is grateful for the support of the *Kepler* Fellowship for the Study of Planet−Bearing Stars. Funding for this Discovery mission is provided by NASA's Science Mission Directorate.

REFERENCES

Audard, M., Güdel, M., Drake, J. J., & Kashyap, V. L. 2000, ApJ, 541, 396

Basri, G., et al. 2010, ApJ, 713, L155

Basri, G., et al. 2010b, in prep.

Benz, A. O.,& Güdel, M. 2010, ARA&A, 48

Bochanski, J. J., Hawley, S. L., Covey, K. R., West, A. A., Reid, I. N., Golimowski, D. A., & Ivezić, Ž. 2010, AJ, 139, 2679

Caldwell, D. A., et al. 2010, ApJ, 713, L92

Charbonneau, P., McIntosh, S. W., Liu, H.-L., & Bogdan, T. J. 2001, Sol. Phys., 203, 321

Covey, K. R., et al. 2008, ApJS, 178, 339

Covey, K. R., et al. 2007, AJ, 134, 2398

Donati, J.-F., et al. 2008, MNRAS, 390, 545

Güdel, M., Audard, M., Kashyap, V. L., Drake, J. J., & Guinan, E. F. 2003, ApJ, 582, 423

Haisch, B., Strong, K. T., & Rodono, M. 1991, ARA&A, 29, 275

Hawley, S. L., Gizis, J. E., & Reid, I. N. 1996, AJ, 112, 2799

Hawley, S. L., et al. 2003, ApJ, 597, 535

Hawley, S. L., Walkowicz, L. M., Allred, J. C., & Valenti, J. A. 2007, PASP, 119, 67

Hawley, S. L. & Pettersen, B. R. 1991, ApJ, 378, 725l. 2004, AJ, 128, 426

Jenkins, J. M., et al. 2010, ApJ, 713, L120

Johns-Krull, C. M., & Valenti, J. A. 1996, ApJ, 459, L95

Koch, D. G., et al. 2010, ApJ, 713, L79

Kowalski, A. F., Hawley, S. L., Hilton, E. J., Becker, A. C., West, A. A., Bochanski, J. J., & Sesar, B. 2009, AJ, 138, 633

Kowalski, A. F., Hawley, S. L., Holtzman, J. A., Wisniewski, J. P., & Hilton, E. J. 2010, ApJ, 714, L98

Latham, D. W., Brown, T. M., Monet, D. G., Everett, M., Esquerdo, G. A., & Hergenrother, C. W. 2005, Bulletin of the American Astronomical Society, 37, 1340

Lacy, C. H., Moffett, T. J., & Evans, D. S. 1976, ApJS, 30, 85

Lu, E. T., & Hamilton, R. J. 1991, ApJ, 380, L89

Osten, R. A., Hawley, S. L., Allred, J. C., Johns-Krull, C. M., & Roark, C. 2005, ApJ, 621, 398

Pickles, A. J. 1998, PASP, 110, 863

Potts, H., Hudson, H., Fletcher, L., & Diver, D. 2010, arXiv:1004.1039

Reiners, A., & Basri, G. 2009, A&A, 496, 787

Saar, S. H., & Linsky, J. L. 1985, ApJ, 299, L47

Segura, A., Walkowicz, L., Meadows, V., Kasting, J., & Hawley, S. 2010, arXiv:1006.0022

Shakhovskaia, N. I. 1989, Sol. Phys., 121, 375

Tarter, J. C., et al. 2007, Astrobiology, 7, 30

Tyson, J. A. 2006, Nature, 442, 364

Walkowicz, L. M. 2008, Ph.D. Thesis,

Walkowicz, L. M., & Hawley, S. L. 2009, AJ, 137, 3297

Walkowicz, L. M., Johns-Krull, C. M., & Hawley, S. L. 2008, ApJ, 677, 593

Watanabe, K., Krucker, S., Hudson, H., Shimizu, T., Masuda, S., & Ichimoto, K. 2010, ApJ, 715, 651

Welsh, B. Y., et al. 2007, ApJS, 173, 673

West, A. A., Hawley, S. L., Bochanski, J. J., Covey, K. R., Reid, I. N., Dhital, S., Hilton, E. J., & Masuda, M. 2008, AJ, 135, 785

West, A. A., et al. 2004, AJ, 128, 426

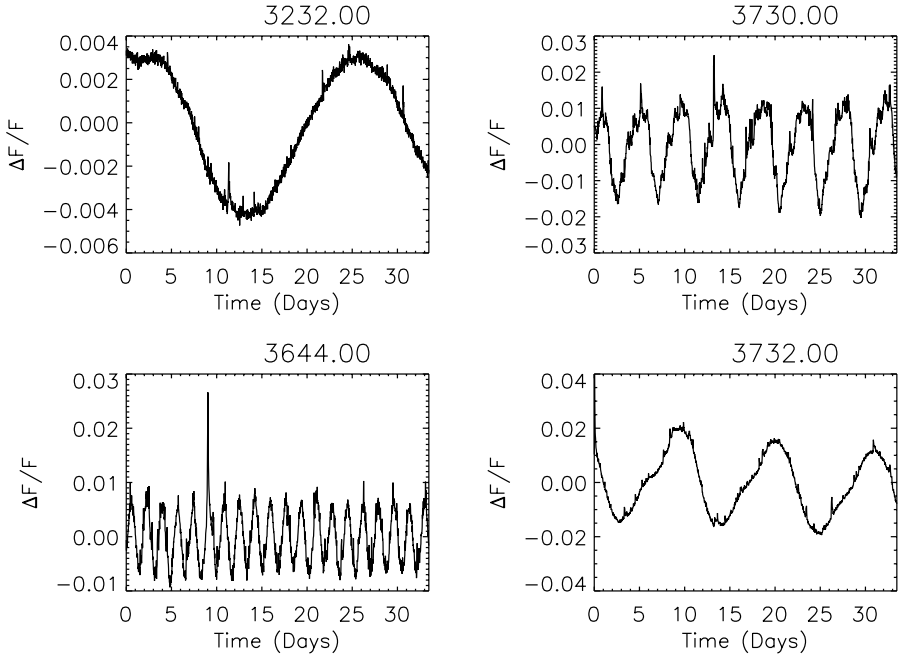

(a) Example lightcurves of four flaring M dwarfs.

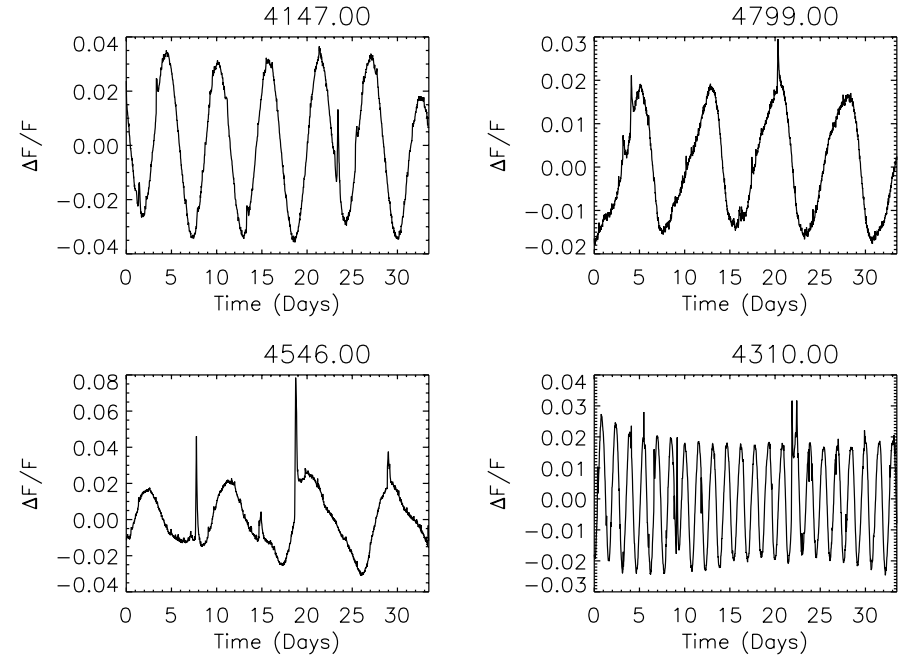

(b) Example lightcurves of four flaring K dwarfs.

Fig. 1.—: Four example flaring M dwarf (top) and K dwarf (bottom) lightcurves from Quarter 1. The effective temperature of the star is listed above each plot.

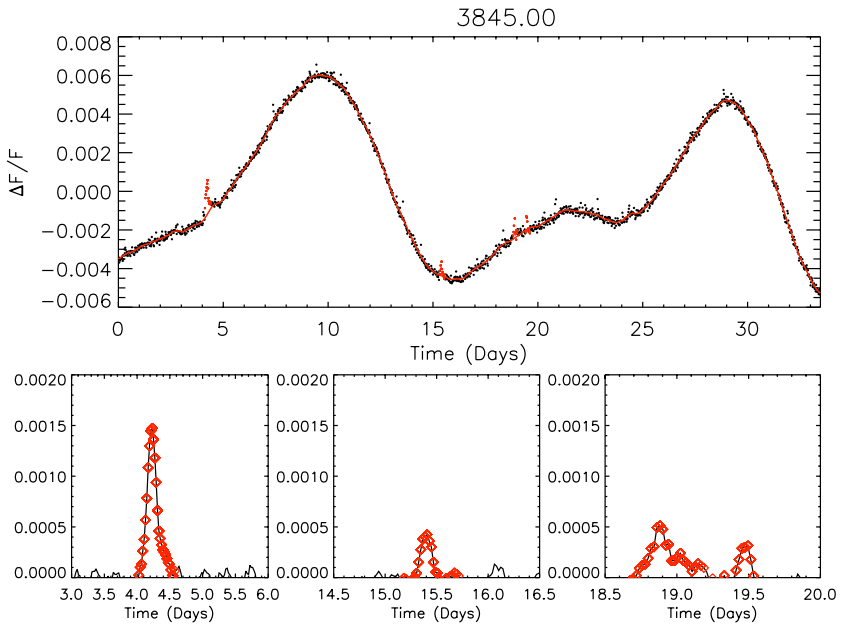

(a) Detail of subtracted lightcurve for an example flaring M dwarf.

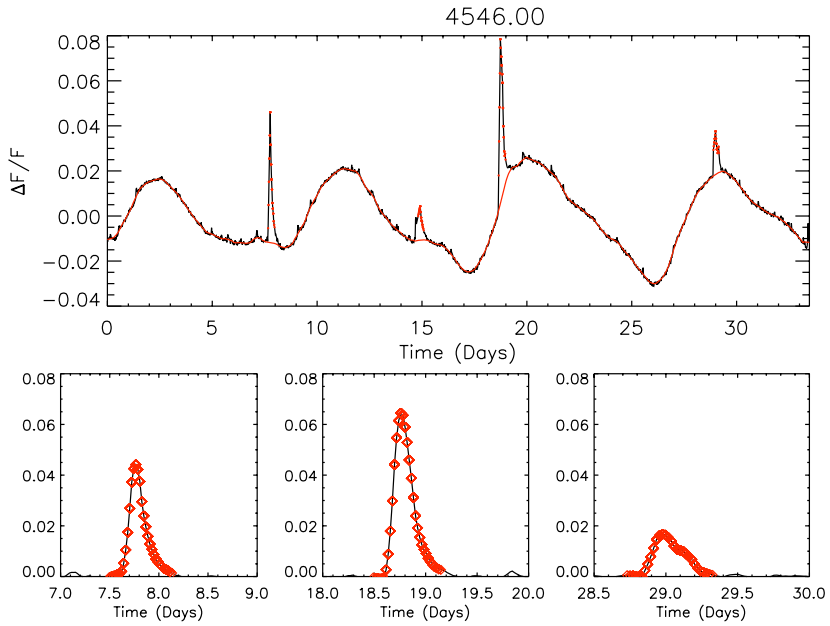

(b) Detail of subtracted lightcurve for an example flaring K dwarf.

Fig. 2.—: Two example lightcurves for one of the flaring M dwarfs (top) and K dwarfs (bottom). In the top panel of each subfigure, the full lightcurve is shown, with the "continuum", or fit to the quiescent variability, overplotted in a solid red line. Points which meet the flare criteria outline in the previous section are marked with red points overlying the data. In the bottom panels, three example flares from each lightcurve are shown at an expanded scale, where the quiescent stellar variability has been subtracted.

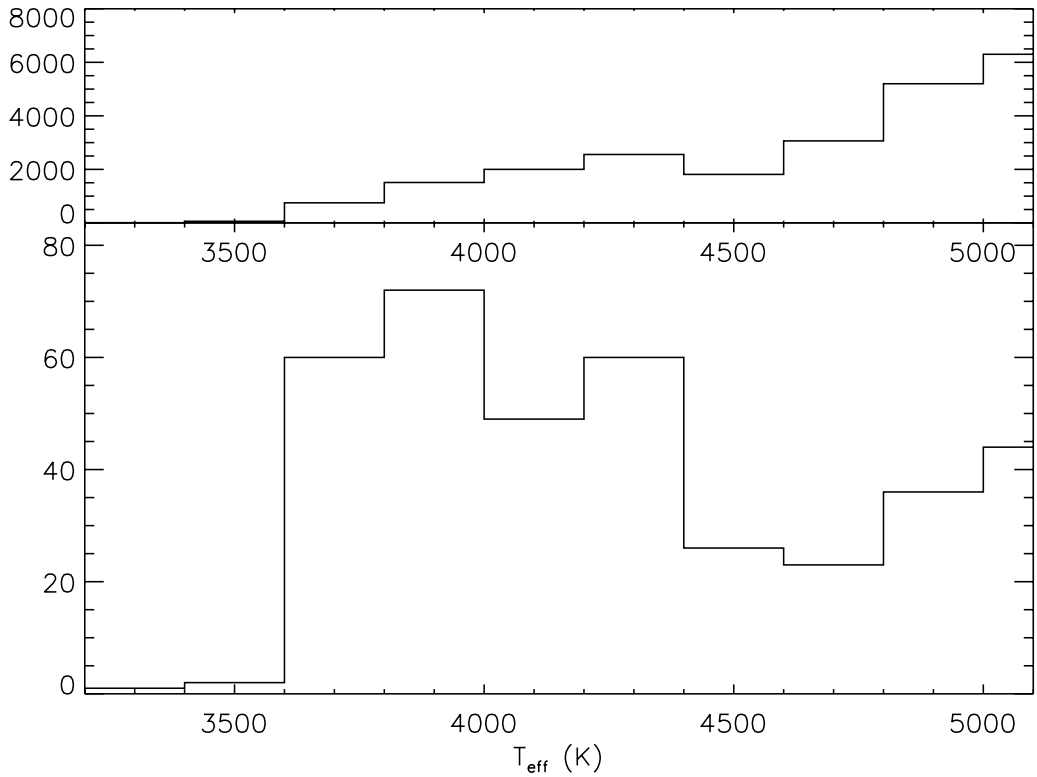

Fig. 3.—: In the upper panel,we show a histogram of the effective temperature distribution of the entire cool dwarf sample, while the effective temperature distribution of the flare stars is shown below. The number of stars found to flare increases with decreasing effective temperature, partly due to the increasing contrast of white light flares.

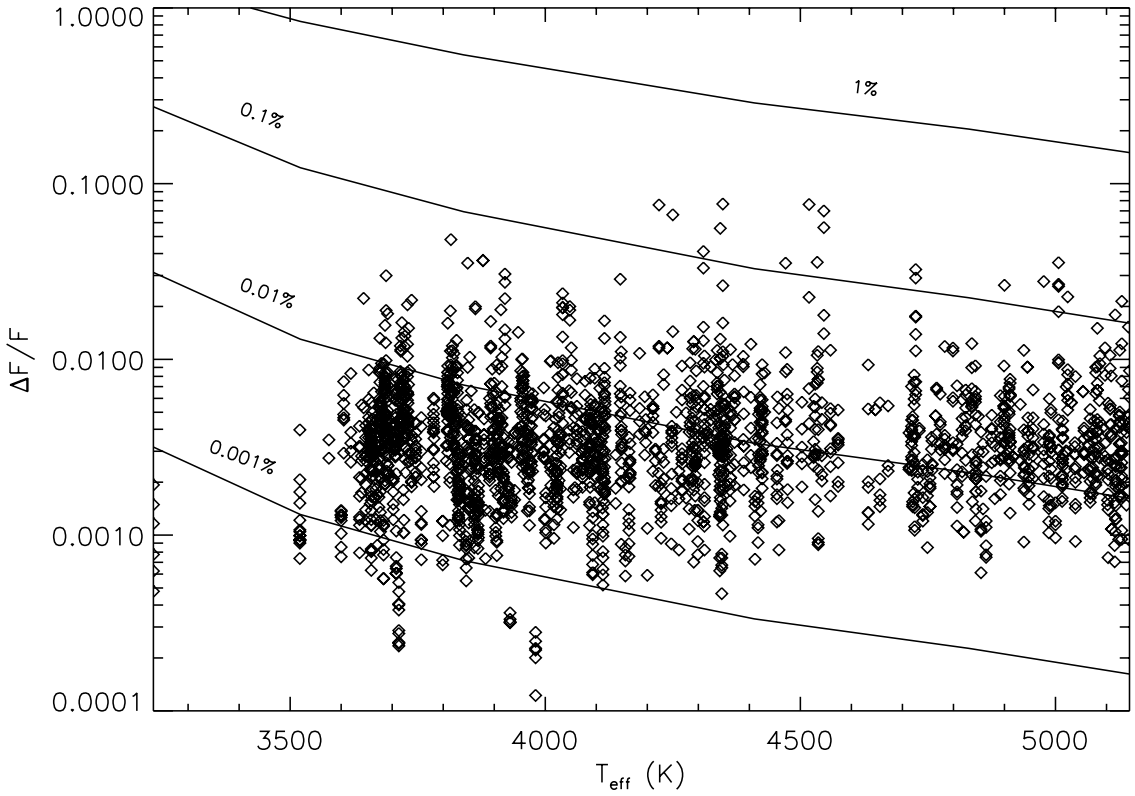

Fig. 4.—: Maximum brightness enhancement for all flares observed versus effective temperature. The data are overplotted with lines of the expected brightness change for a 10,000 K blackbody superimposed on the star at various filling factors: 0.001%, 0.01%, 0.1% and 1% (see the related text for a more complete explanation). The distribution of peak brightness change is more or less flat, as it is possible to detect smaller flares on the M dwarfs due to enhanced contrast between the flare emission and photosphere.

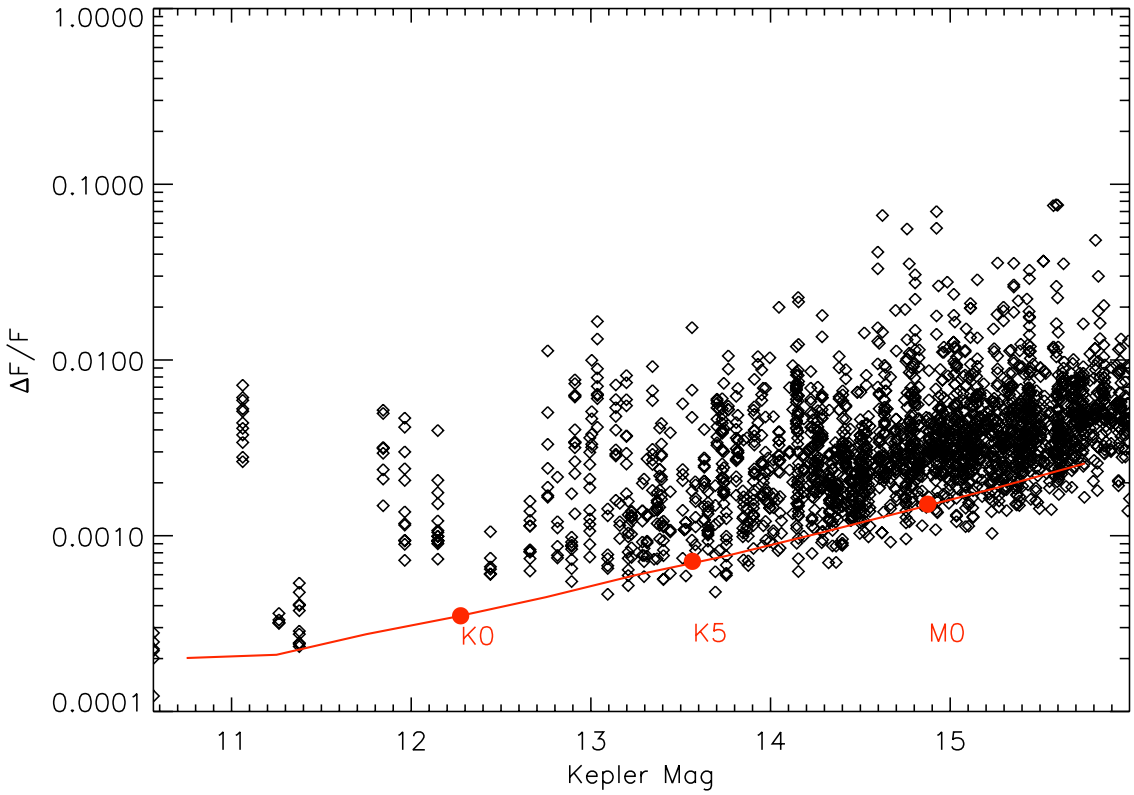

Fig. 5.—: Flare peak height as a function of Kepler magnitude, with our detection threshold overplotted (at least three consecutive points in the lightcurve must lie above this threshold to be tagged as a potential flare). As three red circles, we show where K0, K5 and M0 dwarfs would intersect this threshold if these stars were at a distance of 200 pc. At a given distance, intrinsically more luminous stars are brighter and therefore less noisy, such that the detection threshold is lower. As a result, although the emission from flares on hotter, more luminous stars has lower contrast with their photospheres, one can actually detect a smaller flare on them at a given distance because of their relatively lower noise.

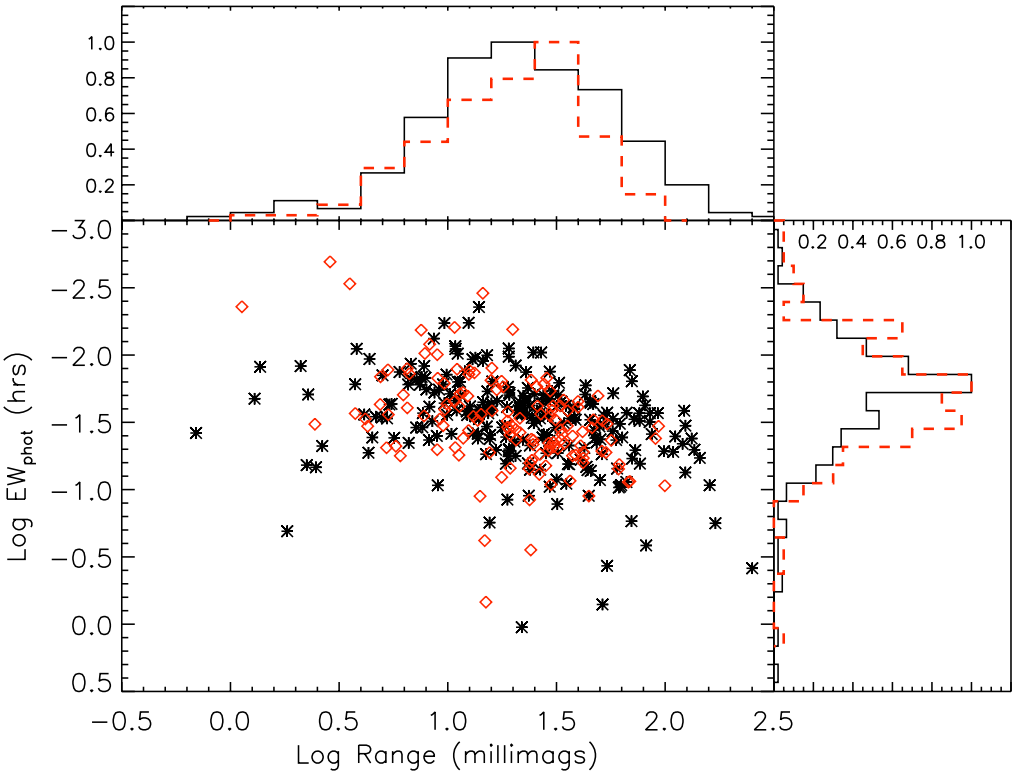

Fig. 6.—: In the center panel we show the variability range versus the photometric equivalent width for the M dwarfs (red diamonds) and the K dwarfs (black asterisks). At top and right we show normalized histograms of these quantities, with the M dwarfs shown as a red dashed line and the K dwarfs as a solid black line. The two samples are roughly comparable in range, with the K dwarfs being slightly more variable in quiescence than the M dwarfs, while the M dwarfs have a somewhat higher photometric equivalent width than the K dwarfs.

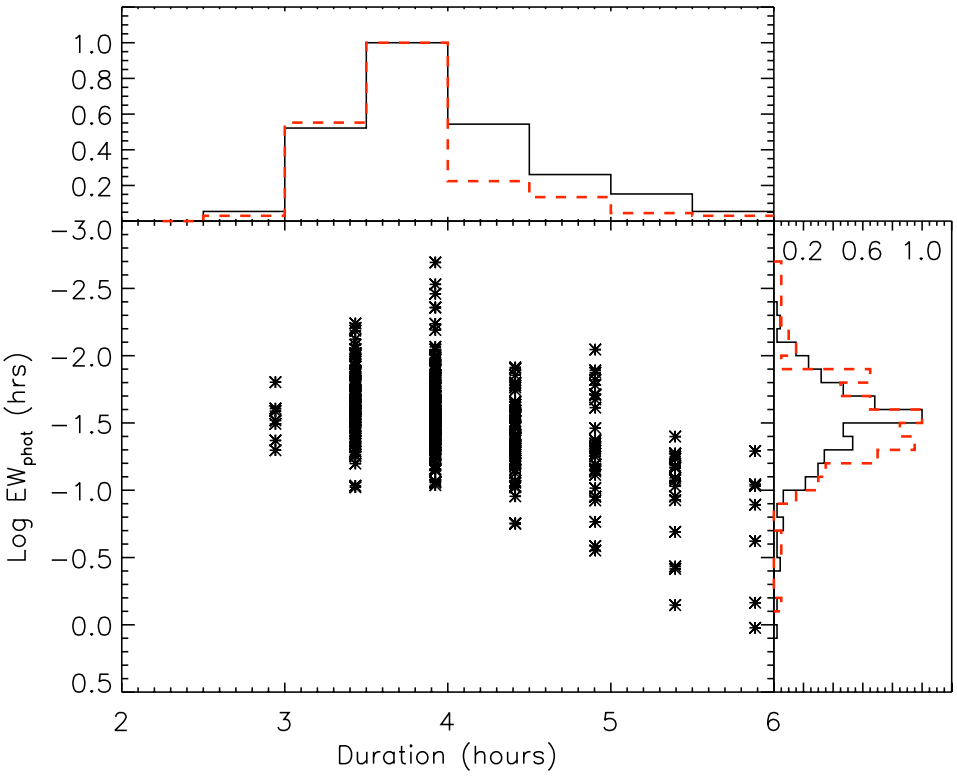

Fig. 7.—: Here we show the median duration of flares versus the photometric equivalent width in the central panel. It is evident that longer duration flares tend to have a higher photometric equivalent width, which is to be expected as photometric equivalent width is a time-integrated quantity. In the top and right histogram panels, we show the duration and photometric equivalent widths separated into M dwarfs (red dashed line) and K dwarfs (black solid line). While the M dwarfs tend to have shorter duration flares, they also tend to have higher photometric equivalent widths than the K dwarfs, implying that they release relatively more energy in a given amount of time.

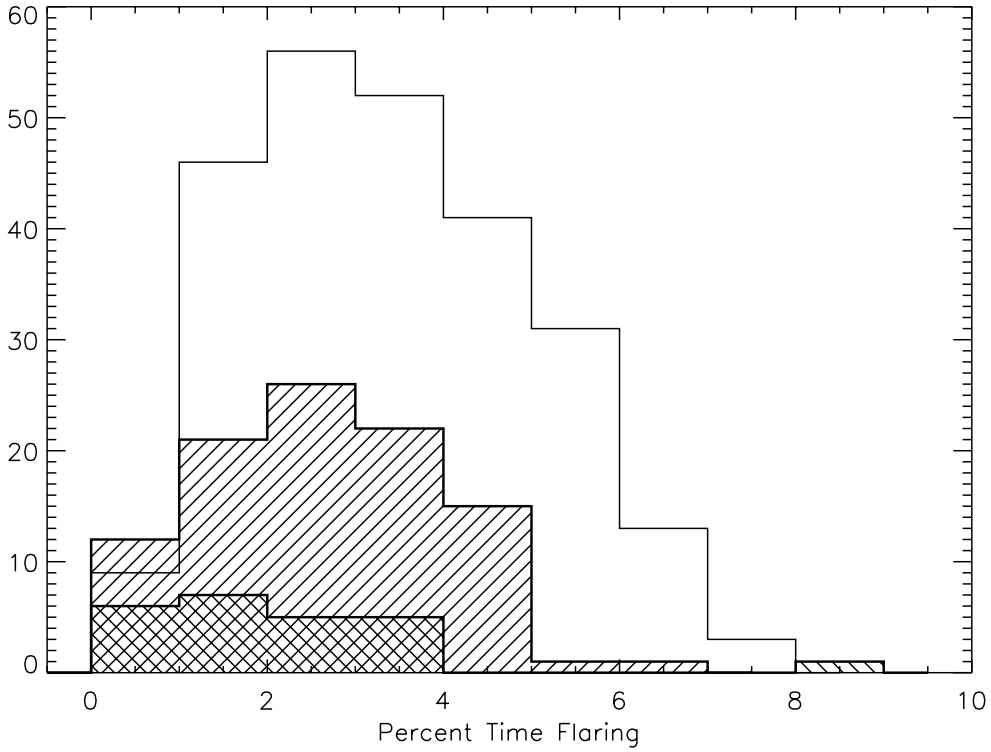

Fig. 8.—: In this figure we show histograms of the percentage of time spent flaring binned by the median flare duration (cross hatched: 5 to 6 hour median duration, diagonal filled: 4 to 5 hour median duration, no fill: median duration less than 4 hours.). The stars which have the longest median flares tend to spend the least amount of time flaring overall, implying that some stars may release the majority of the energy in less frequent long duration events, while others flare more frequently for shorter amounts of time.

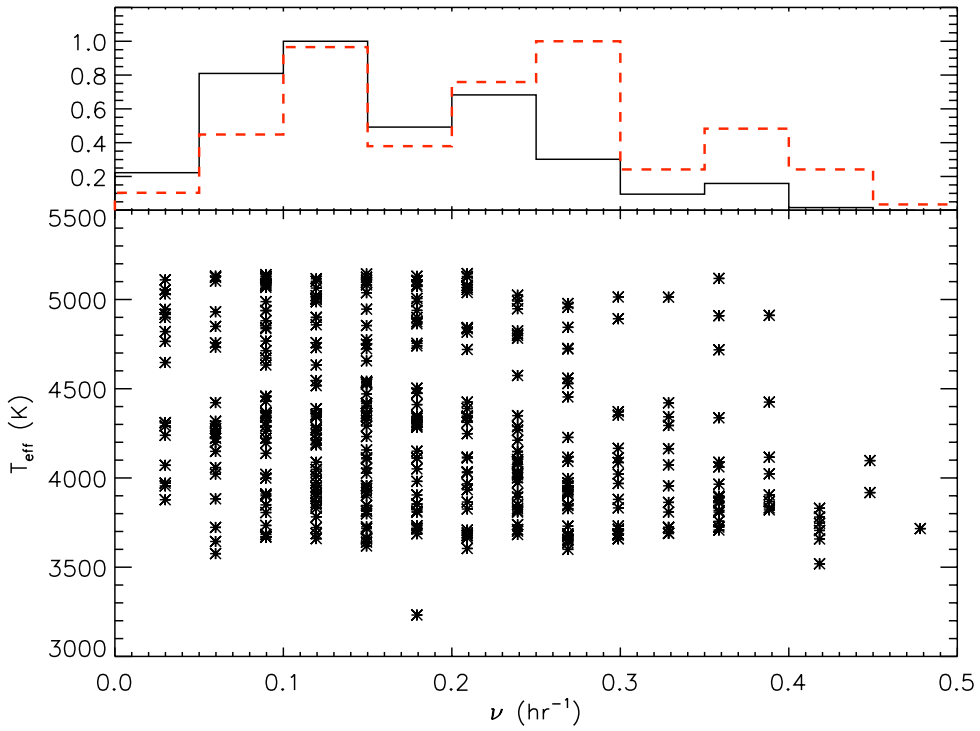

Fig. 9.—: In this figure we plot the flare frequency as a function of temperature in the lower panel, with normalized histograms for the flare frequency of the M dwarfs (red dashed line) and the K dwarfs (black solid line) plotted above. While the two samples have roughly the same amount of stars that flare in the 0.1-0.25 hr^{-1} range, the M dwarfs dominate the population that flares most frequently, while the K dwarfs dominate those who flare least frequently.

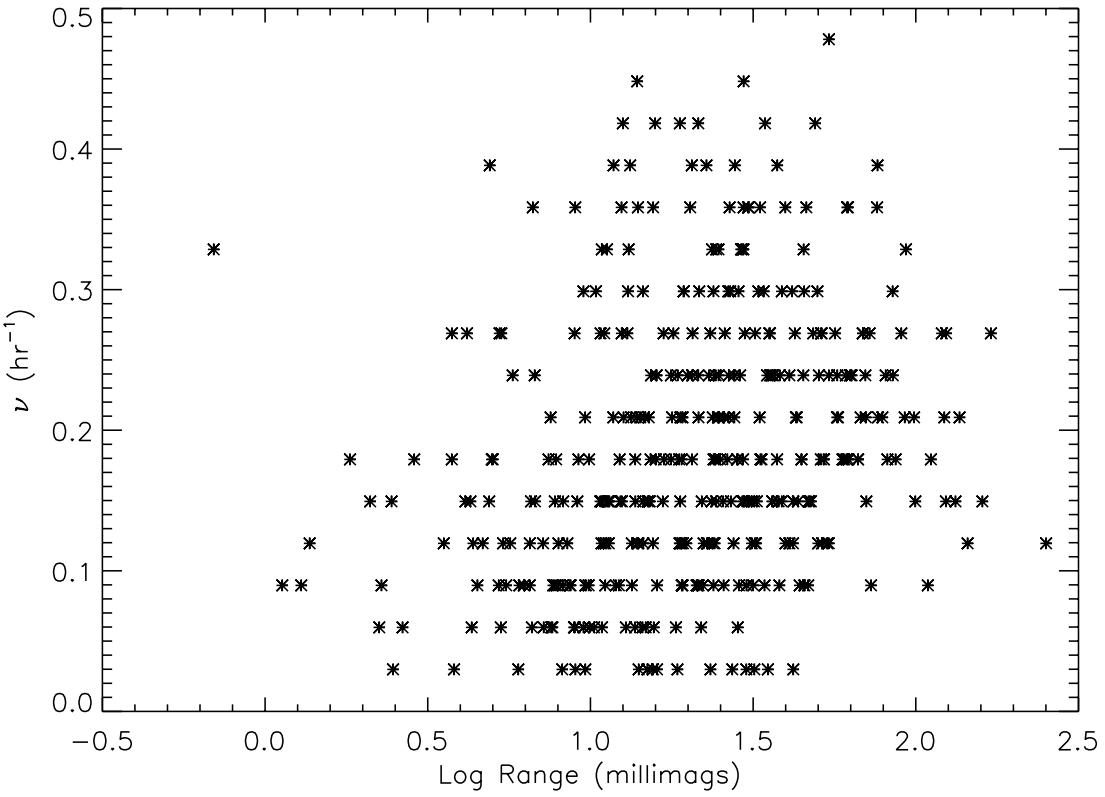

Fig. 10.—: Here we show the distribution of flare frequency with the variability range. There is a wide spread of range with flare frequency, though it does seem that stars that are somewhat more variable in quiescence tend (weakly) to flare more often.

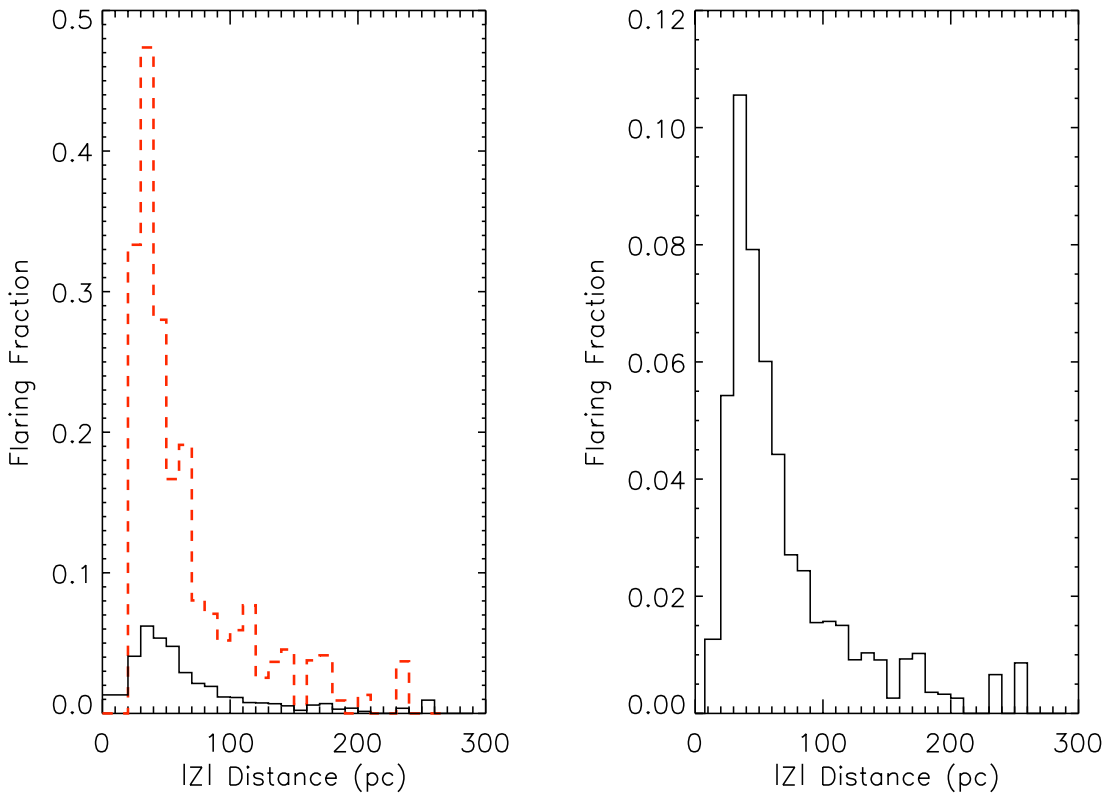

Fig. 11.—: At left we show the flaring fraction of the M dwarfs (red dashed line) and K dwarfs (solid black line) as a function of the distance above the Galactic plane, while at right we show the flare fraction as a function of distance for the entire flare sample.

Table 1. KIC parameters of Stars with Detected Flares

Kepler ID	RA (J2000)	Dec (J2000)	r	J	Kp	g − r	2MASS ID	Teff (deg K)	Logg (cm/s/s)
892376	19 24 15.34	+36 38 08.9	14.093	11.555	13.960	1.383	19241533+3638089	3813	4.471
1569863	19 22 30.36	+37 08 33.7	15.974	13.278	15.856	1.432	19223036+3708336	3809	4.448
1873543	19 30 20.30	+37 23 43.7	14.716	11.939	14.444	1.352	19302029+3723437	3702	4.520
2158047	19 23 50.11	+37 34 42.2	13.937	12.598	13.974	0.662	19235011+3734422	5124	4.306
2300039	19 23 09.62	+37 39 39.7	15.775	12.791	15.427	1.407	19230963+3739397	3644	4.294
2437317	19 20 52.34	+37 45 50.7	14.517	12.878	14.623	1.226	19205233+3745506	4250	4.696
2438151	19 21 08.42	+37 44 55.0	15.323	13.570	15.433	1.076	19210841+3744550	4403	4.576
2441562	19 24 08.52	+37 47 16.9	15.688	13.211	15.558	1.421	19240851+3747169	3806	4.460
2557669	19 07 40.75	+37 52 41.4	14.863	12.388	14.746	1.407	19074075+3752413	3782	4.358
2713086	19 25 47.04	+37 56 58.3	15.062	12.849	15.020	1.282	19254703+3756583	4034	4.287
2716857	19 29 04.51	+37 54 30.5	15.585	13.766	15.604	1.084	19290451+3754305	4248	4.372
2834564	19 06 29.54	+38 04 49.2	14.753	12.019	14.509	1.390	19062955+3804492	3648	4.358
3102749	19 10 26.40	+38 14 54.6	14.327	12.217	14.286	1.236	19102641+3814546	4058	4.639
3109825	19 18 58.99	+38 12 23.7	14.309	11.875	14.185	1.382	19185898+3812236	3832	4.383
3112828	19 22 05.69	+38 15 37.0	14.774	12.903	14.821	1.122	19220568+3815370	4288	4.339
3220938	19 08 58.22	+38 19 57.1	15.283	13.744	15.297	0.722	19085821+3819570	4956	4.440
3222610	19 11 21.10	+38 22 29.4	14.434	12.340	14.419	1.209	19112110+3822294	4097	4.415
3327068	19 07 17.23	+38 25 06.8	14.909	13.384	14.924	0.728	19071723+3825068	4875	4.452
3342210	19 25 50.33	+38 26 23.1	14.375	12.962	14.437	0.756	19255033+3826231	5038	4.248
3439126	19 20 37.73	+38 31 27.8	15.120	13.021	15.104	1.250	19203773+3831277	4088	4.322
3441906	19 23 54.94	+38 34 58.7	13.895	12.534	13.930	0.678	19235494+3834587	5087	4.290
3449953	19 32 07.54	+38 31 06.7	13.666	10.933	13.404	1.393	19320753+3831066	3683	4.353
3534259	19 13 29.50	+38 40 25.5	14.713	13.217	14.773	0.809	19132948+3840254	4843	4.400
3539331	19 19 44.42	+38 38 25.5	14.616	12.762	14.597	1.011	19194441+3838255	4310	4.538
3631401	19 07 49.56	+38 46 20.8	15.877	13.820	15.868	1.209	19074956+3846208	4107	4.541
3632538	19 09 37.20	+38 42 41.7	15.568	14.048	15.600	0.814	19093720+3842417	4647	4.767
3634755	19 12 51.46	+38 45 51.0	13.172	11.663	13.198	0.730	19125144+3845510	4723	4.392
3646734	19 26 55.51	+38 44 38.1	15.208	12.359	14.920	1.351	19265550+3844381	3726	4.469
3750393	19 29 25.01	+38 49 50.8	15.029	13.599	15.178	1.211	19292500+3849507	4730	4.607
3763058	19 41 43.56	+38 53 50.0	14.414	12.320	14.361	1.322	19414356+3853500	3928	4.605
3765091	19 43 14.90	+38 52 28.4	14.605	12.926	14.635	0.951	19431490+3852284	4425	4.445
3836862	19 08 24.58	+38 56 47.4	15.390	13.476	15.383	1.067	19082457+3856474	4312	4.488
3859512	19 35 23.52	+38 54 51.2	14.955	13.022	14.948	1.133	19352352+3854512	4211	4.563
3861049	19 36 53.62	+38 59 28.3	15.545	13.730	15.532	0.967	19365360+3859283	4430	4.515
3861725	19 37 32.06	+38 54 13.4	15.835	13.890	15.806	1.116	19373207+3854133	4239	4.615
3934090	18 58 00.02	+39 04 57.5	15.114	12.755	15.036	1.359	18580001+3904575	3905	4.206

Table 1—Continued

Kepler ID	RA (J2000)	Dec (J2000)	r	J	Kp	g − r	2MASS ID	Teff (deg K)	Logg (cm/s/s)
3940372	19 08 17.45	+39 02 34.6	16.296	13.160	15.860	1.246	19081745+3902346	3605	4.209
3942324	19 11 22.78	+39 05 33.5	13.377	11.736	13.393	0.895	19112278+3905335	4454	4.515
3945784	19 16 00.55	+39 02 53.1	13.411	11.958	13.442	0.697	19160054+3902530	4854	4.444
3967523	19 39 34.15	+39 03 58.8	15.449	13.939	15.480	0.815	19393415+3903588	4824	4.465
4043389	19 09 31.70	+39 10 51.5	11.695	8.840	11.377	1.353	19093170+3910515	3713	4.385
4147537	19 15 34.70	+39 17 54.6	15.310	13.701	15.361	0.887	19153470+3917546	4672	4.519
4158372	19 27 17.64	+39 13 02.4	13.749	11.742	13.740	1.207	19271763+3913024	4116	4.380
4171937	19 39 41.54	+39 17 49.5	14.966	13.567	14.999	0.677	19394153+3917495	5014	4.829
4243462	19 01 45.65	+39 22 56.6	13.117	11.551	13.161	0.868	19014565+3922566	5000	4.529
4243508	19 01 51.10	+39 21 43.7	15.019	13.643	15.049	0.637	19015110+3921436	5126	4.628
4248763	19 10 08.42	+39 18 55.1	13.103	10.984	13.036	1.110	19100840+3918551	4116	4.520
4274517	19 38 00.62	+39 19 50.1	14.795	13.044	14.828	1.090	19380061+3919500	4294	4.568
4349043	19 05 52.49	+39 26 02.6	14.739	12.868	14.760	1.047	19055248+3926025	4343	4.441
4355503	19 15 28.44	+39 29 46.1	15.246	12.698	15.068	1.413	19152845+3929460	3658	4.699
4375336	19 36 49.58	+39 29 20.4	15.031	13.330	15.042	0.943	19364958+3929203	4425	4.478
4455709	19 16 13.73	+39 30 38.6	15.621	13.910	15.645	0.994	19161372+3930385	4356	4.580
4466498	19 28 54.74	+39 33 07.3	14.215	12.510	14.273	1.076	19285475+3933073	4268	4.688
4484377	19 45 51.22	+39 30 48.8	14.512	13.111	14.533	0.665	19455121+3930488	5139	4.305
4554781	19 18 47.86	+39 38 40.5	14.103	11.782	14.016	1.155	19184785+3938404	4001	4.536
4644174	19 14 10.66	+39 47 57.6	14.582	12.394	14.514	1.231	19141064+3947575	4022	4.548
4649344	19 20 27.70	+39 44 39.1	14.944	13.416	14.984	0.749	19202769+3944391	4977	4.223
4650327	19 21 30.82	+39 43 13.5	15.242	13.605	15.245	0.737	19213082+3943135	4799	4.430
4661946	19 35 04.22	+39 47 30.6	15.174	13.782	15.219	0.737	19350423+3947305	5068	4.486
4669417	19 42 08.98	+39 44 18.1	14.146	12.663	14.154	0.652	19420897+3944181	5024	4.502
4673009	19 45 07.37	+39 47 34.2	14.025	12.595	14.053	0.753	19450736+3947341	4749	4.573
4725913	18 55 53.54	+39 51 58.1	14.534	12.592	14.533	1.136	18555354+3951581	4232	4.427
4726192	18 56 24.70	+39 48 20.8	14.772	12.476	14.699	1.342	18562468+3948208	3908	4.513
4741455	19 20 43.85	+39 50 52.1	15.228	12.964	15.167	1.358	19204384+3950521	3898	4.445
4758595	19 39 58.87	+39 50 53.0	12.361	9.798	12.148	1.399	19395886+3950530	3519	4.410
4819423	19 05 10.90	+39 55 18.5	15.554	13.580	15.525	1.044	19051090+3955185	4296	4.535
4819766	19 05 44.95	+39 58 10.0	15.820	13.323	15.675	1.397	19054495+3958099	3828	4.444
4832949	19 23 50.71	+39 57 53.2	14.899	13.005	14.949	1.258	19235071+3957532	4071	4.417
4844804	19 37 19.78	+39 59 08.1	15.642	13.496	15.635	1.301	19371978+3959080	4010	4.515
4907159	19 04 14.59	+40 04 35.2	14.384	12.497	14.382	1.066	19041458+4004351	4312	4.435
4913533	19 14 44.47	+40 01 12.4	15.661	14.131	15.693	0.893	19144447+4001124	4526	4.705
4919569	19 21 53.18	+40 01 44.6	15.747	13.653	15.735	1.266	19215317+4001446	4047	4.529

Table 1—Continued

Kepler ID	RA (J2000)	Dec (J2000)	r	J	Kp	g − r	2MASS ID	Teff (deg K)	Logg (cm/s/s)
4929016	19 33 06.91	+40 05 06.6	13.725	11.563	13.702	1.293	19330692+4005066	3973	4.490
4933923	19 38 14.98	+40 00 59.1	14.265	12.922	14.290	0.625	19381498+4000591	5130	4.523
4939265	19 43 09.94	+40 00 44.5	13.790	11.503	13.731	1.431	19430993+4000445	3781	4.462
4990413	18 56 19.30	+40 06 54.3	14.198	12.250	14.209	1.149	18561929+4006542	4216	4.444
5008689	19 24 18.89	+40 10 50.1	14.494	12.766	14.545	1.043	19241888+4010501	4362	4.469
5015542	19 32 25.18	+40 07 11.6	15.767	13.682	15.741	1.183	19322516+4007116	4089	4.551
5016904	19 33 56.57	+40 10 54.6	15.476	12.566	15.151	1.434	19335656+4010546	3660	4.376
5079590	18 57 53.30	+40 12 48.8	15.385	13.458	15.331	0.941	18575329+4012488	4337	4.552
5131463	19 57 26.54	+40 17 00.8	15.363	13.367	15.365	1.213	19572655+4017008	4138	4.661
5167100	18 58 30.22	+40 21 40.1	13.946	12.554	13.986	0.637	18583021+4021400	5068	4.457
5182822	19 22 00.24	+40 22 13.1	15.716	13.464	15.673	1.333	19220024+4022130	3955	4.356
5217339	19 55 24.84	+40 18 20.5	14.031	12.678	14.106	0.650	19552484+4018205	5021	4.560
5268904	19 19 46.15	+40 28 24.8	14.571	11.580	14.236	1.425	19194614+4028248	3661	4.271
5288534	19 41 58.08	+40 27 57.7	15.610	13.400	15.625	1.364	19415808+4027577	3956	4.389
5360082	19 24 19.99	+40 33 59.9	14.755	13.055	14.772	0.927	19241999+4033599	4471	4.330
5371494	19 37 26.18	+40 33 50.8	14.350	12.516	14.393	···	19372617+4033508	4247	4.307
5397422	19 59 38.28	+40 31 54.2	14.584	12.282	14.502	1.300	19593828+4031541	3967	4.375
5428088	18 56 32.76	+40 37 52.5	14.935	12.394	14.781	1.384	18563275+4037524	3821	4.283
5437459	19 13 08.30	+40 38 18.1	15.271	13.028	15.230	1.310	19130830+4038180	3965	4.400
5461756	19 42 00.34	+40 38 30.2	14.045	11.654	13.905	1.342	19420033+4038302	3861	4.611
5513266	18 56 08.57	+40 46 44.8	16.140	13.800	15.947	1.019	18560856+4046448	4051	4.585
5516671	19 03 05.86	+40 46 00.8	15.705	12.910	15.446	1.344	19030585+4046008	3818	4.402
5607395	19 10 49.51	+40 53 09.3	15.681	13.400	15.593	1.312	19104951+4053093	3975	4.467
5648400	19 55 10.54	+40 50 42.4	13.541	11.843	13.583	1.030	19551055+4050423	4312	4.543
5693747	19 11 35.42	+40 57 36.2	15.627	14.157	15.691	0.816	19113543+4057362	4899	4.643
5694127	19 12 09.91	+40 59 04.5	15.001	12.962	14.965	1.171	19120990+4059044	4149	4.600
5702236	19 22 55.46	+40 57 58.9	14.297	12.929	14.322	0.634	19225545+4057589	5079	4.597
5709193	19 31 50.23	+40 54 11.3	15.530	13.326	15.477	1.352	19315023+4054113	3940	4.523
5722668	19 45 49.44	+40 59 54.1	14.251	12.162	14.241	1.252	19454944+4059540	4055	4.394
5729898	19 51 45.05	+40 56 05.4	15.809	13.724	15.734	1.152	19514505+4056054	4117	4.605
5732553	19 53 59.35	+40 58 16.3	15.358	13.819	15.396	0.711	19535933+4058163	5086	4.499
5770769	18 56 32.26	+41 05 40.4	15.227	13.615	15.264	0.880	18563224+4105404	4533	4.468
5784256	19 18 50.16	+41 00 21.3	14.740	13.349	14.796	0.793	19185015+4100212	4843	4.923
5855096	18 53 31.22	+41 10 29.5	15.102	12.993	15.088	1.293	18533121+4110295	4022	4.432
5858361	19 00 03.94	+41 09 46.0	14.494	11.743	14.231	1.396	19000393+4109460	3636	4.288
5859365	19 02 01.44	+41 10 53.4	15.822	13.377	15.679	1.396	19020142+4110533	3808	4.631

Table 1—Continued

Kepler ID	RA (J2000)	Dec (J2000)	r	J	Kp	g − r	2MASS ID	Teff (deg K)	Logg (cm/s/s)
5952853	19 17 40.42	+41 17 27.7	13.264	11.372	13.296	1.168	19174040+4117277	4157	4.375
5962532	19 30 11.50	+41 15 37.5	15.419	13.944	15.433	0.731	19301150+4115375	4909	4.612
5992270	19 58 29.28	+41 12 45.0	14.741	12.967	14.782	1.145	19582927+4112450	4222	4.565
6021431	18 53 15.91	+41 21 42.0	13.980	12.237	14.042	1.069	18531590+4121420	4262	4.440
6029338	19 08 31.75	+41 20 06.2	15.111	13.705	15.126	0.696	19083175+4120062	4931	4.564
6033083	19 14 53.86	+41 23 55.0	15.894	14.553	15.957	0.716	19145385+4123550	5076	4.985
6038882	19 22 31.06	+41 20 22.5	14.667	12.528	14.648	1.313	19223104+4120225	3971	4.389
6045059	19 30 32.52	+41 22 46.7	14.785	13.189	14.819	0.718	19303252+4122467	4939	4.442
6100469	18 50 13.63	+41 24 51.7	15.148	13.631	15.192	0.829	18501363+4124516	4765	4.453
6116129	19 17 51.96	+41 27 36.3	14.076	11.740	13.996	1.362	19175196+4127362	3852	4.420
6119605	19 22 04.78	+41 27 54.5	14.250	12.978	14.288	0.628	19220478+4127544	5117	4.681
6141300	19 46 33.41	+41 27 11.2	15.711	13.865	15.744	1.105	19463340+4127111	4312	4.384
6146804	19 51 36.89	+41 29 57.7	14.273	12.730	14.290	0.803	19513688+4129576	4633	4.395
6224062	19 47 54.79	+41 35 30.2	14.568	12.157	14.454	1.380	19475480+4135302	3830	4.493
6263016	18 50 50.28	+41 38 19.9	15.436	13.628	15.450	0.983	18505029+4138199	4352	4.336
6290789	19 34 32.78	+41 36 41.3	15.109	13.083	15.103	1.249	19343278+4136412	4087	4.519
6290811	19 34 33.96	+41 37 23.6	15.656	12.954	15.411	1.371	19343395+4137235	3689	4.550
6310265	19 53 35.33	+41 39 32.9	16.161	13.259	15.855	1.387	19533533+4139329	3730	4.398
6356144	19 16 46.97	+41 44 16.5	14.805	12.509	14.749	1.387	19164697+4144165	3863	4.341
6380533	19 45 54.22	+41 44 02.8	14.672	13.275	14.744	0.720	19455421+4144028	5131	4.380
6425928	19 01 05.40	+41 51 29.4	14.633	12.176	14.522	1.259	19010540+4151293	3947	4.485
6431497	19 11 14.28	+41 51 15.0	14.977	13.426	15.035	0.911	19111428+4151150	4740	4.356
6510289	19 11 04.78	+41 59 38.4	15.524	14.095	15.579	0.720	19110477+4159384	5129	4.615
6521729	19 26 20.93	+41 57 22.1	15.678	13.948	15.677	0.951	19262093+4157220	4455	4.488
6522124	19 26 51.55	+41 55 57.0	15.306	13.948	15.385	0.801	19265156+4155569	5102	4.561
6542087	19 48 35.76	+41 55 21.1	15.326	13.257	15.314	1.300	19483576+4155210	4030	4.469
6547641	19 53 30.65	+41 57 10.3	14.097	12.640	14.124	0.792	19533065+4157102	4633	4.626
6548898	19 54 30.48	+41 58 49.3	15.099	12.148	14.751	1.381	19543047+4158492	3665	4.285
6606167	19 27 20.81	+42 03 06.9	14.809	13.208	14.867	0.867	19272081+4203068	4720	4.421
6608436	19 30 02.35	+42 04 58.3	14.937	13.492	14.988	0.697	19300235+4204582	5097	4.439
6610837	19 32 48.02	+42 00 58.0	15.598	12.595	15.249	1.400	19324802+4200580	3640	4.263
6620003	19 42 29.33	+42 05 34.4	15.733	13.394	15.686	1.314	19422932+4205343	3955	4.444
6668646	18 53 44.09	+42 08 27.5	15.361	12.711	15.201	1.391	18534407+4208274	3731	4.528
6668936	18 54 07.01	+42 06 56.0	13.487	11.753	13.528	1.015	18540700+4206559	4310	4.330
6674908	19 04 42.41	+42 11 47.5	14.304	11.817	14.155	1.319	19044240+4211475	3869	4.529
6675714	19 06 03.05	+42 08 02.4	14.673	12.564	14.607	1.208	19060303+4208024	4073	4.604

Table 1—Continued

Kepler ID	RA (J2000)	Dec (J2000)	r	J	Kp	g − r	2MASS ID	Teff (deg K)	Logg (cm/s/s)
6763067	19 07 42.24	+42 14 14.9	15.838	13.454	15.720	1.388	19074224+4214149	3846	4.622
6766663	19 13 19.92	+42 17 41.8	13.901	11.698	13.846	1.346	19131991+4217418	3903	4.504
6767913	19 15 10.70	+42 12 39.0	15.433	13.952	15.449	0.735	19151070+4212390	4881	4.613
6783369	19 34 16.22	+42 16 49.4	14.803	11.986	14.524	1.393	19341623+4216494	3677	4.304
6843185	18 57 58.75	+42 23 58.3	15.186	13.067	15.151	1.162	18575874+4223583	4147	4.433
6846570	19 04 22.39	+42 20 10.9	14.811	12.255	14.696	1.291	19042239+4220108	3913	4.459
6863726	19 28 05.21	+42 18 55.1	14.191	11.497	13.957	1.386	19280520+4218551	3671	4.366
6871896	19 37 29.18	+42 22 44.8	14.621	12.394	14.553	1.299	19372917+4222448	3969	4.543
6928206	18 56 42.10	+42 27 40.8	14.485	11.948	14.345	1.366	18564210+4227408	3832	4.331
6949412	19 28 17.42	+42 26 38.1	15.796	13.275	15.631	1.366	19281741+4226380	3848	4.443
7017604	19 04 16.08	+42 31 05.9	15.036	13.470	15.086	0.793	19041608+4231059	4807	4.498
7018323	19 05 37.03	+42 35 30.8	15.456	12.957	15.308	1.364	19053703+4235308	3830	4.626
7031565	19 24 32.40	+42 31 22.4	15.474	14.002	15.487	0.748	19243239+4231223	4837	4.620
7107430	19 13 47.45	+42 36 54.5	13.208	11.236	13.208	1.203	19134744+4236545	4113	4.404
7133807	19 44 44.18	+42 37 52.1	15.618	13.397	15.553	1.118	19444419+4237521	4113	4.536
7188204	19 11 06.10	+42 44 10.6	15.338	13.858	15.393	0.799	19110608+4244105	4836	4.617
7191311	19 15 50.50	+42 47 06.0	14.651	12.266	14.535	1.405	19155048+4247060	3746	4.626
7192199	19 17 06.94	+42 43 49.7	15.788	13.708	15.797	1.309	19170693+4243496	4027	4.435
7215890	19 44 27.89	+42 44 31.5	14.002	11.557	13.876	1.383	19442788+4244314	3799	4.396
7218950	19 47 15.31	+42 45 38.4	14.126	12.795	14.156	0.629	19471531+4245384	5130	4.580
7281399	19 26 20.04	+42 49 48.2	15.932	14.214	15.989	1.094	19262003+4249481	4293	4.728
7293120	19 40 13.22	+42 53 38.5	15.251	13.611	15.314	1.063	19401323+4253385	4343	4.643
7347797	19 06 27.26	+42 55 26.4	15.273	13.547	15.289	0.980	19062727+4255264	4363	4.435
7347999	19 06 46.63	+42 56 14.4	14.369	12.756	14.400	0.866	19064662+4256144	4535	4.464
7381180	19 47 18.41	+42 56 45.3	15.125	13.250	15.147	1.069	19471840+4256452	4371	4.287
7422811	18 54 17.28	+43 05 20.7	15.963	13.329	15.741	1.349	18541728+4305206	3809	4.897
7456455	19 40 19.37	+43 01 07.6	14.472	12.929	14.482	0.803	19401936+4301076	4754	4.507
7461212	19 44 51.89	+43 04 16.1	13.702	12.070	13.765	0.619	19445188+4304161	5107	4.483
7465605	19 48 33.67	+43 04 26.4	13.677	11.426	13.652	1.386	19483366+4304263	3868	4.259
7509281	19 00 38.14	+43 09 43.1	16.177	13.458	15.951	1.414	19003813+4309431	3676	4.531
7509473	19 01 00.02	+43 09 38.0	13.230	11.544	13.287	1.013	19010002+4309380	4299	4.483
7509496	19 01 02.30	+43 09 05.2	14.459	12.490	14.471	1.218	19010231+4309052	4113	4.361
7551695	19 51 19.56	+43 10 28.1	15.340	13.173	15.297	1.246	19511955+4310280	4048	4.385
7592133	19 03 47.09	+43 17 20.8	15.227	12.182	14.882	1.460	19034709+4317208	3654	4.236
7670700	19 08 54.07	+43 20 39.5	15.521	12.622	15.233	1.410	19085407+4320395	3722	4.370
7677767	19 20 44.33	+43 23 29.1	12.649	9.978	12.441	1.375	19204433+4323291	3708	4.427

Table 1—Continued

Kepler ID	RA (J2000)	Dec (J2000)	r	J	Kp	g − r	2MASS ID	Teff (deg K)	Logg (cm/s/s)
7692454	19 40 03.00	+43 19 35.3	12.896	10.172	12.661	1.397	19400298+4319352	3659	4.354
7751342	19 24 49.87	+43 29 25.0	15.775	13.272	15.624	1.322	19244986+4329250	3855	4.601
7772109	19 50 12.82	+43 25 07.2	13.471	11.728	13.529	1.128	19501280+4325072	4200	4.476
7830341	19 37 50.88	+43 31 28.2	14.568	12.368	14.500	1.376	19375087+4331282	3880	4.543
7830503	19 38 02.38	+43 33 54.3	15.469	13.989	15.502	0.771	19380236+4333542	4945	4.435
7836762	19 45 31.97	+43 35 42.6	14.307	12.228	14.327	1.321	19453196+4335426	3999	4.470
7849619	19 58 02.71	+43 34 02.1	15.572	13.288	15.519	1.369	19580270+4334020	3878	4.518
7871438	18 51 27.31	+43 40 28.3	14.152	11.659	14.047	1.350	18512731+4340282	3863	4.421
7877209	19 03 52.85	+43 38 27.4	15.827	13.188	15.620	1.433	19035284+4338273	3708	4.472
7885309	19 19 26.76	+43 36 07.5	14.250	12.689	14.264	0.809	19192677+4336074	4574	4.452
7907119	19 47 37.42	+43 40 57.1	14.370	12.186	14.329	1.355	19473742+4340571	3918	4.528
7936309	18 41 39.48	+43 45 53.1	11.001	9.410	11.062	0.904	18413947+4345531	4421	4.413
7937049	18 43 45.96	+43 42 32.3	15.718	14.137	15.740	0.792	18434597+4342322	4774	4.500
7959162	19 25 59.09	+43 43 16.1	13.456	12.130	13.520	0.682	19255909+4343160	5110	4.351
7987934	19 59 27.98	+43 42 38.3	15.750	13.013	15.522	1.412	19592797+4342382	3734	4.514
8004647	18 40 20.90	+43 51 20.1	14.923	13.523	14.935	0.692	18402090+4351200	4900	4.543
8007234	18 47 27.00	+43 48 01.1	16.218	13.352	15.937	1.407	18472701+4348011	3676	4.321
8042251	19 44 59.78	+43 52 55.7	11.287	9.198	11.264	1.320	19445977+4352556	3931	4.422
8104467	19 36 50.57	+43 54 37.5	15.514	13.394	15.477	1.247	19365056+4354375	4088	4.462
8149782	18 59 27.65	+44 02 10.1	15.787	13.596	15.746	1.284	18592765+4402101	4020	4.536
8176468	19 41 37.01	+44 03 43.8	12.958	11.066	12.994	1.167	19413700+4403437	4164	4.421
8196449	20 02 49.06	+44 00 40.5	14.703	11.821	14.402	1.410	20024906+4400404	3706	4.302
8249046	19 47 52.13	+44 09 48.5	15.352	13.955	15.370	0.694	19475213+4409485	5103	4.559
8292758	19 17 16.01	+44 14 36.6	15.152	12.867	15.113	1.267	19171599+4414366	4034	4.291
8302555	19 31 35.81	+44 12 10.1	16.225	13.230	15.895	1.410	19313580+4412100	3679	4.301
8316096	19 48 48.07	+44 13 00.9	14.743	12.816	14.754	1.160	19484808+4413009	4227	4.420
8321490	19 53 59.45	+44 12 22.0	15.504	13.461	15.497	1.242	19535943+4412220	4112	4.463
8343785	18 44 33.91	+44 23 34.9	15.878	13.621	15.801	1.328	18443392+4423349	3954	4.515
8376893	19 43 03.17	+44 23 53.8	16.073	13.919	15.975	1.162	19430317+4423538	4078	4.574
8416925	19 02 29.30	+44 28 16.3	14.858	13.189	14.926	1.044	19022930+4428162	4422	4.565
8456954	19 59 03.94	+44 26 13.1	15.451	12.711	15.127	1.144	19590394+4426130	3619	4.621
8479655	18 57 43.25	+44 35 55.8	12.724	11.458	12.760	0.587	18574324+4435558	5126	4.602
8482565	19 04 35.21	+44 33 07.1	15.904	13.964	15.937	1.131	19043521+4433070	4289	4.435
8487242	19 14 35.69	+44 34 02.4	14.247	12.721	14.263	0.766	19143569+4434023	4718	4.458
8491152	19 21 15.67	+44 35 28.4	15.327	13.797	15.371	0.746	19211568+4435283	4948	4.390
8540644	18 50 08.28	+44 39 12.7	13.680	12.022	13.714	0.923	18500827+4439126	4458	4.439

Table 1—Continued

Kepler ID	RA (J2000)	Dec (J2000)	r	J	Kp	g − r	2MASS ID	Teff (deg K)	Logg (cm/s/s)
8546579	19 03 04.06	+44 39 16.6	13.796	12.217	13.850	0.952	19030406+4439165	4411	4.616
8560255	19 27 33.82	+44 37 08.5	14.547	13.054	14.620	0.905	19273381+4437085	4820	4.300
8572338	19 45 02.33	+44 36 49.3	14.946	13.515	14.965	0.739	19450233+4436492	4783	4.750
8604575	18 47 58.66	+44 42 14.6	15.601	13.548	15.575	1.097	18475865+4442146	4223	4.534
8617530	19 16 09.70	+44 45 23.5	14.205	12.814	14.285	0.810	19160969+4445235	4938	4.529
8620472	19 20 56.52	+44 47 56.8	15.066	13.420	15.148	1.086	19205651+4447568	4318	4.656
8651471	19 59 55.85	+44 42 47.9	13.473	12.198	13.511	0.684	19595584+4442478	5103	4.283
8684857	19 20 39.60	+44 53 41.7	15.322	13.926	15.390	0.853	19203960+4453417	4917	4.565
8776565	19 56 28.39	+44 54 59.3	15.228	12.460	15.028	1.434	19562839+4454592	3692	4.532
8845205	20 00 49.46	+45 01 05.3	14.915	12.275	14.708	1.449	20004946+4501053	3576	4.444
8881943	19 21 56.14	+45 11 11.4	14.756	13.321	14.785	0.659	19215613+4511114	5079	4.642
8935140	18 55 31.66	+45 15 47.3	15.714	13.743	15.682	1.065	18553164+4515473	4284	4.578
8947255	19 19 04.22	+45 15 49.1	15.553	12.695	15.261	1.371	19190422+4515490	3691	4.413
8959288	19 36 24.62	+45 16 14.2	14.739	13.329	14.787	0.732	19362462+4516141	5013	4.309
9002074	18 52 20.69	+45 19 13.6	16.231	13.490	15.987	1.414	18522069+4519135	3715	4.453
9030716	19 39 32.98	+45 18 14.0	14.836	13.086	14.844	0.981	19393297+4518140	4348	4.416
9048551	19 58 01.15	+45 18 06.0	13.411	11.233	13.383	1.271	19580115+4518060	4017	4.468
9048949	19 58 25.82	+45 23 26.5	11.765	10.439	11.844	0.704	19582581+4523265	4991	4.426
9051905	20 01 36.29	+45 21 03.5	14.923	13.090	14.960	1.094	20013629+4521035	4257	4.326
9117167	20 01 01.73	+45 29 57.8	13.544	11.701	13.581	1.159	20010173+4529578	4149	4.321
9159012	19 34 21.70	+45 33 55.3	13.701	11.846	13.754	1.228	19342168+4533553	4093	4.445
9163591	19 41 00.12	+45 33 45.0	15.921	14.218	15.896	1.028	19410011+4533450	4324	4.586
9179906	20 00 03.86	+45 31 40.5	16.094	13.085	15.722	1.435	20000387+4531405	3686	4.307
9180393	20 00 36.29	+45 32 22.6	15.511	14.007	15.503	0.824	20003627+4532226	4946	4.634
9214598	19 21 21.24	+45 40 51.0	13.814	12.342	13.869	0.800	19212123+4540510	4724	4.667
9220002	19 30 13.75	+45 38 06.6	15.101	13.611	15.138	0.666	19301374+4538066	5145	4.382
9224698	19 37 17.81	+45 39 03.7	15.590	14.176	15.605	0.734	19371780+4539036	5073	4.494
9238899	19 54 45.67	+45 40 58.5	14.894	12.598	14.826	1.335	19544567+4540584	3915	4.379
9239775	19 55 44.42	+45 41 02.7	14.896	12.897	14.919	1.085	19554441+4541027	4282	4.484
9267818	19 00 27.70	+45 47 06.1	15.257	12.682	15.089	1.411	19002769+4547061	3732	4.346
9269688	19 04 51.50	+45 43 40.3	14.919	13.080	14.929	1.071	19045149+4543402	4343	4.436
9346592	19 34 04.42	+45 48 51.2	13.900	11.851	13.910	1.250	19340442+4548511	4062	4.350
9349698	19 38 41.93	+45 51 54.7	12.891	11.492	12.911	0.659	19384193+4551547	4911	4.537
9395205	19 10 01.58	+45 57 10.9	14.706	12.477	14.630	1.347	19100158+4557109	3891	4.598
9407581	19 33 03.58	+45 56 55.3	15.643	13.067	15.462	1.414	19330357+4556552	3679	4.578
9425635	19 56 35.81	+45 54 45.7	15.054	12.753	14.963	1.359	19563580+4554457	3849	4.530

Table 1—Continued

Kepler ID	RA (J2000)	Dec (J2000)	r	J	Kp	g − r	2MASS ID	Teff (deg K)	Logg (cm/s/s)
9428095	19 59 37.82	+45 56 04.8	16.198	13.214	15.860	1.379	19593783+4556047	3684	4.316
9450669	18 58 15.31	+46 03 12.9	15.436	13.749	15.441	0.774	18581531+4603128	4726	4.431
9468935	19 33 51.94	+46 03 06.7	14.538	12.333	14.495	1.338	19335194+4603066	3934	4.420
9474589	19 41 59.40	+46 01 04.7	13.792	11.449	13.693	1.413	19415940+4601047	3232	4.624
9480850	19 49 59.90	+46 04 20.4	15.087	13.327	15.127	1.106	19495989+4604203	4342	4.597
9508099	18 47 31.61	+46 07 29.9	15.899	13.965	15.926	1.023	18473161+4607298	4367	4.454
9530263	19 33 44.11	+46 08 50.8	15.281	13.351	15.300	1.233	19334412+4608508	4110	4.553
9540467	19 48 23.23	+46 10 16.7	12.066	9.638	11.964	1.386	19482323+4610167	3757	4.457
9570305	18 50 01.44	+46 12 50.7	15.499	13.878	15.503	0.640	18500142+4612507	5109	4.468
9576197	19 03 32.28	+46 17 23.4	14.593	13.228	14.641	0.677	19033227+4617233	5082	4.551
9579266	19 10 40.68	+46 16 24.0	15.870	14.502	15.925	0.768	19104068+4616240	5031	4.599
9581885	19 16 31.68	+46 13 52.2	15.584	12.935	15.379	1.382	19163168+4613522	3738	4.512
9588880	19 28 39.84	+46 13 39.5	14.736	12.487	14.703	1.399	19283982+4613394	3865	4.343
9596620	19 40 36.10	+46 16 23.7	15.483	13.407	15.537	1.423	19403609+4616236	3910	4.296
9613610	20 01 13.94	+46 17 07.3	14.575	12.971	14.671	0.817	20011394+4617073	4758	4.524
9631366	18 48 39.58	+46 18 31.9	14.114	11.740	13.972	1.357	18483957+4618318	3827	4.587
9637196	19 02 49.27	+46 19 22.5	14.134	12.372	14.155	0.989	19024926+4619225	4342	4.489
9659036	19 42 48.31	+46 22 31.7	15.350	13.093	15.295	1.285	19424832+4622317	3973	4.543
9697509	19 01 12.60	+46 29 50.7	15.643	13.858	15.563	0.721	19011260+4629507	4858	4.468
9713986	19 33 32.76	+46 26 02.8	15.715	13.765	15.700	1.065	19333277+4626027	4291	4.561
9765275	19 18 03.34	+46 33 21.7	15.378	13.522	15.403	1.089	19180334+4633216	4348	4.406
9784213	19 47 56.83	+46 33 48.1	15.179	13.701	15.241	0.786	19475683+4633481	5082	4.233
9838763	19 39 47.57	+46 36 15.7	15.375	13.930	15.399	0.726	19394755+4636157	4899	4.639
9880382	19 06 24.31	+46 45 06.5	15.583	13.996	15.605	0.761	19062430+4645064	4817	4.516
9892651	19 30 25.42	+46 47 24.9	15.964	13.473	15.809	1.386	19302541+4647249	3815	4.746
9909614	19 53 48.14	+46 46 15.6	15.228	13.599	15.272	0.926	19534813+4646156	4656	4.270
9941718	19 08 03.46	+46 48 40.8	15.783	13.051	15.601	1.426	19080345+4648407	3724	4.453
9945771	19 17 26.74	+46 53 32.5	14.905	12.454	14.805	1.304	19172674+4653324	3921	4.375
9969320	19 53 33.19	+46 52 21.9	15.541	13.971	15.595	0.931	19533319+4652219	4757	4.376
10002792	19 11 28.13	+46 58 59.1	12.986	11.201	13.005	0.994	19112813+4658590	4334	4.448
10011038	19 26 07.32	+46 59 46.1	15.270	13.541	15.339	1.095	19260732+4659460	4363	4.577
10056727	18 51 52.15	+47 04 01.4	14.903	13.500	14.960	0.716	18515215+4704013	5056	4.366
10065745	19 10 48.53	+47 04 42.5	16.104	13.196	15.834	1.451	19104853+4704425	3719	4.431
10070247	19 19 27.41	+47 04 51.7	15.582	13.666	15.591	0.978	19192740+4704516	4348	4.505
10134498	19 16 53.28	+47 06 20.8	15.716	13.699	15.699	1.137	19165327+4706208	4195	4.617
10139305	19 24 34.56	+47 11 07.7	14.596	13.141	14.605	0.700	19243456+4711076	4899	4.480

Table 1—Continued

Kepler ID	RA (J2000)	Dec (J2000)	r	J	Kp	g − r	2MASS ID	Teff (deg K)	Logg (cm/s/s)
10165244	19 58 06.17	+47 10 09.8	14.911	12.522	14.803	1.242	19580616+4710097	4025	4.486
10188460	18 49 28.37	+47 12 08.4	13.471	11.105	13.369	1.347	18492836+4712083	3850	4.467
10196750	19 07 06.94	+47 15 48.0	15.840	13.994	15.819	1.007	19070692+4715479	4389	4.574
10208370	19 28 19.49	+47 13 08.4	14.963	13.301	14.993	0.910	19281948+4713084	4475	4.428
10288161	19 47 48.24	+47 22 55.2	15.094	13.154	15.113	1.200	19474824+4722551	4150	4.533
10317398	18 40 55.82	+47 27 03.5	15.035	13.275	15.035	0.924	18405583+4727034	4388	4.327
10319112	18 45 27.91	+47 28 37.6	15.222	13.702	15.284	0.738	18452791+4728375	4988	4.475
10320656	18 49 23.11	+47 28 55.7	12.988	10.691	12.893	1.365	18492311+4728557	3845	4.560
10363074	19 58 17.35	+47 24 05.9	15.535	12.848	15.319	1.397	19581735+4724059	3711	4.527
10397709	19 15 15.14	+47 33 28.0	15.323	13.875	15.354	0.765	19151514+4733280	5006	4.200
10422252	19 51 39.07	+47 33 49.7	13.582	12.317	13.631	0.703	19513906+4733497	5118	4.229
10449542	18 46 10.97	+47 37 12.9	15.773	13.868	15.778	1.048	18461097+4737129	4351	4.500
10471960	19 30 08.69	+47 36 07.3	15.623	13.041	15.439	1.392	19300868+4736072	3814	4.498
10513641	18 42 50.38	+47 42 09.5	15.793	13.692	15.778	1.139	18425037+4742095	4185	4.443
10518758	18 55 42.29	+47 45 12.2	15.177	12.925	15.127	1.341	18554228+4745122	3919	4.378
10528093	19 15 32.23	+47 45 34.2	13.506	12.198	13.563	0.625	19153224+4745341	5143	4.526
10536761	19 30 11.33	+47 44 01.8	14.930	11.990	14.605	1.365	19301133+4744018	3687	4.306
10548015	19 46 43.66	+47 44 57.7	15.387	13.910	15.425	0.773	19464367+4744576	4849	4.691
10622511	19 57 16.39	+47 48 06.7	13.432	10.875	13.226	1.380	19571639+4748067	3600	4.603
10658494	19 15 28.80	+47 54 59.6	15.032	13.176	15.073	1.178	19152878+4754596	4166	4.490
10727657	19 21 44.18	+48 00 02.6	14.101	12.483	14.146	0.943	19214417+4800026	4417	4.521
10753072	19 55 36.02	+48 05 35.7	15.685	12.910	15.444	1.417	19553603+4805356	3664	4.391
10779266	18 52 31.46	+48 07 47.7	15.210	13.688	15.239	0.869	18523145+4807476	4542	4.678
10790838	19 16 53.64	+48 06 11.7	16.162	13.481	15.941	1.377	19165364+4806116	3816	4.470
10793290	19 21 00.60	+48 11 40.8	15.943	14.176	15.998	1.145	19210060+4811408	4276	4.735
10801273	19 33 54.98	+48 08 14.7	10.540	8.545	10.565	1.289	19335498+4808147	3981	4.356
10818065	19 55 20.57	+48 08 07.7	15.380	13.612	15.387	0.914	19552056+4808076	4559	4.541
10857583	19 20 31.01	+48 12 30.5	15.198	12.715	15.083	1.457	19203100+4812305	3717	4.316
10865206	19 34 05.86	+48 14 30.6	13.927	12.303	13.951	0.883	19340586+4814305	4474	4.451
10872868	19 44 59.30	+48 12 41.6	15.415	12.557	15.125	1.422	19445931+4812415	3674	4.403
10905040	18 52 28.94	+48 22 05.2	14.648	13.166	14.700	0.710	18522895+4822052	4938	4.485
10938188	19 55 44.90	+48 20 03.4	14.677	11.926	14.415	1.405	19554490+4820034	3657	4.332
10960823	18 52 42.38	+48 28 36.8	15.877	13.243	15.695	1.417	18524238+4828368	3722	4.300
10975238	19 26 33.34	+48 25 33.3	15.088	12.808	15.026	1.371	19263334+4825333	3893	4.386
10990728	19 52 09.86	+48 27 34.0	15.459	13.579	15.483	1.137	19520986+4827339	4309	4.378
10991547	19 53 25.18	+48 26 34.2	15.692	14.310	15.747	0.720	19532516+4826341	5125	4.710

Table 1—Continued

Kepler ID	RA (J2000)	Dec (J2000)	r	J	Kp	g − r	2MASS ID	Teff (deg K)	Logg (cm/s/s)
11017875	19 01 01.30	+48 31 55.3	15.715	13.295	15.596	1.376	19010129+4831553	3850	4.564
11032573	19 32 58.15	+48 33 43.3	15.642	13.746	15.640	1.071	19325815+4833433	4346	4.571
11037498	19 41 24.31	+48 33 25.0	14.803	12.631	14.754	1.293	19412431+4833250	4011	4.455
11047115	19 55 26.06	+48 31 30.7	15.395	13.505	15.383	1.029	19552605+4831306	4349	4.516
11068661	18 50 17.50	+48 37 43.2	15.517	13.900	15.598	0.980	18501750+4837432	4517	4.565
11081377	19 21 33.24	+48 36 51.8	13.370	11.185	13.313	1.341	19213322+4836518	3905	4.554
11124203	18 56 47.14	+48 46 04.7	14.477	11.811	14.287	1.385	18564713+4846047	3725	4.524
11128748	19 08 59.47	+48 47 17.7	14.243	12.484	14.323	1.090	19085946+4847177	4291	4.527
11190713	19 27 59.59	+48 49 03.3	13.126	11.480	13.139	0.821	19275959+4849033	4529	4.352
11190969	19 28 33.53	+48 52 27.7	12.779	11.460	12.814	0.682	19283352+4852276	4864	4.701
11190988	19 28 36.24	+48 53 43.0	14.313	12.939	14.365	0.717	19283624+4853429	5116	4.210
11192887	19 32 25.51	+48 52 01.5	14.656	13.255	14.668	0.656	19322550+4852015	5039	4.444
11196403	19 38 47.81	+48 51 30.8	13.880	11.628	13.818	1.269	19384780+4851308	3997	4.292
11244150	19 27 24.48	+48 57 11.3	15.082	12.621	14.945	1.318	19272448+4857112	3910	4.382
11251134	19 40 21.72	+48 56 31.3	15.760	14.278	15.844	0.930	19402171+4856313	4767	4.709
11342883	19 11 26.18	+49 07 16.3	13.329	11.571	13.343	1.006	19112619+4907162	4268	4.448
11465987	19 47 03.05	+49 22 00.6	14.966	13.563	15.025	0.746	19470305+4922006	5006	4.622
11493667	18 54 42.79	+49 27 11.2	15.128	12.942	15.073	1.342	18544280+4927112	3958	4.400
11515276	19 42 16.15	+49 28 07.0	16.144	13.632	15.993	1.404	19421615+4928069	3826	4.526
11521274	19 51 26.66	+49 24 52.8	14.699	11.840	14.449	1.417	19512666+4924527	3668	4.201
11550428	19 06 46.49	+49 31 16.2	15.210	12.189	14.882	1.414	19064648+4931162	3659	4.257
11569291	19 46 09.34	+49 33 17.9	15.388	13.718	15.407	0.989	19460933+4933179	4418	4.583
11612409	19 31 01.34	+49 40 44.2	14.201	11.707	14.061	1.386	19310135+4940442	3723	4.348
11658934	19 20 42.43	+49 43 53.2	14.838	13.102	14.896	1.030	19204243+4943531	4340	4.360
11662738	19 29 33.72	+49 45 18.3	14.942	13.361	14.957	0.843	19293372+4945183	4535	4.465
11663521	19 31 11.90	+49 42 35.9	13.035	11.330	13.094	1.004	19311189+4942359	4346	4.407
11717648	19 37 14.69	+49 50 17.7	14.362	12.278	14.375	1.290	19371467+4950176	4023	4.328
11721444	19 43 42.07	+49 51 24.5	14.721	13.154	14.739	0.783	19434206+4951245	4713	4.459
11808734	19 15 28.46	+50 01 37.5	15.534	12.939	15.346	1.385	19152845+5001374	3809	4.425
11824222	19 46 28.46	+50 01 19.2	14.486	13.148	14.497	0.695	19462846+5001192	4987	4.570
11859900	19 17 42.89	+50 09 17.6	14.713	12.637	14.692	1.225	19174288+5009176	4103	4.419
11870769	19 40 44.64	+50 07 58.9	16.121	13.361	15.825	1.364	19404465+5007589	3688	4.583
11873179	19 44 48.24	+50 09 40.0	15.055	13.092	15.019	1.042	19444825+5009399	4291	4.569
11958955	19 16 06.43	+50 21 19.6	14.175	12.875	14.246	0.825	19160644+5021195	4844	4.556
11969772	19 39 47.04	+50 21 11.2	14.356	12.922	14.402	0.697	19394704+5021111	4988	4.360
12004872	19 06 15.07	+50 29 22.2	14.410	11.663	14.151	1.381	19061507+5029221	3686	4.436

Table 1—Continued

Kepler ID	RA (J2000)	Dec (J2000)	r	J	Kp	g − r	2MASS ID	Teff (deg K)	Logg (cm/s/s)
12061183	19 24 48.72	+50 35 04.3	15.006	13.353	15.035	0.924	19244873+5035043	4503	4.505
12105694	19 13 44.66	+50 40 46.1	15.870	13.557	15.808	1.373	19134466+5040461	3896	4.406
12117857	19 40 59.38	+50 36 38.8	14.438	13.042	14.483	0.739	19405938+5036388	5054	4.201
12254596	19 17 14.42	+50 56 42.7	13.433	11.147	13.352	1.341	19171441+5056426	3883	4.531
12258055	19 25 19.30	+50 57 27.8	14.324	11.955	14.224	1.288	19251930+5057277	3952	4.347
12303977	19 17 35.59	+51 04 12.7	14.906	13.285	14.924	0.865	19173560+5104127	4546	4.300
12314646	19 41 22.34	+51 04 27.3	14.419	11.567	14.144	1.442	19412234+5104273	3716	4.458
12356051	19 23 21.50	+51 07 05.3	15.780	12.778	15.441	1.407	19232149+5107053	3686	4.314
12401644	19 12 06.65	+51 13 50.5	13.784	12.273	13.809	0.680	19120665+5113505	4892	4.280
12599435	19 14 54.94	+51 39 47.6	14.663	13.173	14.723	0.845	19145492+5139476	4733	4.499
12599998	19 16 11.28	+51 40 57.3	15.358	13.262	15.337	1.106	19161129+5140572	4197	4.500
12735599	19 18 40.25	+51 59 15.0	14.878	13.500	14.911	0.672	19184024+5159149	5064	4.441
12835232	19 21 44.57	+52 10 41.0	15.322	12.935	15.187	1.324	19214456+5210410	3900	4.612

Table 2. Flare Statistics

Kepler ID	#	Log EW_{phot}	Log $\Delta F/F$	Median Duration (hours)	$t_{between}$ (hours)	ν (hours^{-1})	% flaring
892376	5	−3.094	−2.674	4.904	104.46	0.15	2.9
1569863	8	−2.756	−2.296	3.923	125.55	0.24	3.7
1873543	8	−3.186	−2.694	3.433	117.70	0.24	3.5
2158047	2	−2.972	−2.736	4.414	576.25	0.06	0.9
2300039	2	−2.002	−1.653	5.885	15.20	0.06	1.3
2437317	2	−1.357	−1.177	5.885	118.19	0.06	1.5
2438151	5	−2.760	−2.391	4.414	79.94	0.15	2.5
2441562	3	−2.827	−2.491	3.923	93.18	0.09	1.5
2557669	4	−2.693	−2.382	4.904	117.21	0.12	2.1
2713086	7	−2.573	−2.084	3.923	43.65	0.21	3.7
2716857	7	−2.966	−2.447	3.923	35.31	0.21	3.3
2834564	9	−3.122	−2.577	4.414	46.10	0.27	4.6
3102749	2	−2.562	−2.331	5.395	338.39	0.06	1.2
3109825	10	−3.004	−2.621	3.923	50.51	0.30	4.6
3112828	8	−2.791	−2.526	4.414	86.81	0.24	4.2
3220938	9	−2.909	−2.496	3.923	58.36	0.27	4.4
3222610	15	−2.905	−2.540	3.923	37.76	0.45	7.5
3327068	6	−2.951	−2.398	3.923	42.67	0.18	2.9
3342210	5	−2.840	−2.537	4.414	80.43	0.15	2.7
3439126	12	−2.757	−2.475	3.923	51.98	0.36	5.9
3441906	3	−2.455	−2.024	5.395	198.13	0.09	1.6
3449953	8	−3.571	−3.028	3.923	55.42	0.24	3.6
3534259	3	−3.391	−2.678	3.433	65.23	0.09	1.2
3539331	6	−2.334	−1.816	5.395	60.32	0.18	3.7
3631401	5	−2.821	−2.377	3.433	133.40	0.15	2.3
3632538	1	−2.572	−2.286	4.904	0.00	0.03	0.6
3634755	9	−2.721	−2.431	4.414	92.20	0.27	4.8
3646734	5	−2.927	−2.499	3.433	78.47	0.15	2.4
3750393	4	−2.969	−2.682	3.923	115.25	0.12	1.8
3763058	9	−2.966	−2.561	3.923	92.69	0.27	4.6
3765091	13	−2.892	−2.316	3.923	56.40	0.39	6.6
3836862	7	−2.874	−2.467	3.923	53.46	0.21	3.5
3859512	8	−2.948	−2.282	3.923	94.65	0.24	3.8
3861049	3	−2.768	−2.300	3.923	40.21	0.09	1.6
3861725	1	−2.412	−1.935	5.885	0.00	0.03	0.7
3934090	13	−2.763	−2.381	3.923	32.37	0.39	6.3
3940372	7	−2.716	−2.313	3.923	51.00	0.21	3.3
3942324	9	−3.268	−2.665	3.433	59.34	0.27	4.1
3945784	5	−3.174	−2.967	4.414	85.33	0.15	2.6
3967523	8	−2.529	−2.329	4.414	85.33	0.24	4.3
4043389	10	−3.840	−3.426	3.923	58.36	0.30	4.9
4147537	3	−3.007	−2.604	3.433	94.16	0.09	1.5
4158372	13	−2.941	−2.700	3.923	44.14	0.39	6.5
4171937	10	−2.909	−2.540	3.923	48.55	0.30	4.6
4243462	4	−3.253	−2.920	4.904	30.41	0.12	2.2
4243508	3	−2.785	−2.363	4.414	154.48	0.09	1.6
4248763	9	−2.690	−2.150	4.414	26.48	0.27	4.9
4274517	11	−2.899	−2.589	3.923	50.51	0.33	5.1

Table 2—Continued

Kepler ID	#	Log EW_{phot}	Log $\Delta F/F$	Median Duration (hours)	$t_{between}$ (hours)	ν (hours^{-1})	% flaring
4349043	6	−2.436	−1.993	4.414	113.29	0.18	3.1
4355503	14	−2.912	−2.472	3.433	32.86	0.42	6.2
4375336	7	−3.099	−2.544	3.433	84.84	0.21	3.2
4455709	4	−2.888	−2.509	4.414	81.90	0.12	2.0
4466498	4	−3.037	−2.680	3.923	261.40	0.12	1.9
4484377	3	−3.260	−2.699	3.433	21.09	0.09	1.5
4554781	8	−3.206	−2.788	3.433	82.39	0.24	3.7
4644174	10	−2.849	−2.630	3.433	63.76	0.30	4.4
4649344	9	−2.855	−2.515	3.923	30.41	0.27	4.2
4650327	8	−2.570	−2.238	4.904	63.76	0.24	4.4
4661946	7	−3.185	−2.631	3.433	69.15	0.21	3.4
4669417	8	−2.906	−2.140	3.923	70.62	0.24	4.1
4673009	5	−3.315	−2.776	3.923	116.72	0.15	2.6
4725913	5	−2.742	−2.510	3.433	61.79	0.15	2.5
4726192	9	−3.001	−2.623	3.433	57.38	0.27	4.1
4741455	12	−2.820	−2.409	3.923	52.48	0.36	6.0
4758595	14	−3.267	−2.981	3.923	40.71	0.42	7.0
4819423	6	−2.932	−2.232	3.923	60.32	0.18	2.7
4819766	9	−2.685	−2.285	3.923	67.19	0.27	4.6
4832949	1	−2.972	−2.532	4.414	0.00	0.03	0.5
4844804	4	−2.914	−2.420	3.923	286.90	0.12	1.9
4907159	6	−2.749	−2.210	4.414	85.33	0.18	3.2
4913533	5	−2.994	−2.550	3.923	42.18	0.15	2.4
4919569	4	−2.765	−2.405	4.414	173.12	0.12	2.0
4929016	9	−2.761	−2.337	3.923	52.48	0.27	4.5
4933923	3	−3.503	−2.974	3.433	232.95	0.09	1.4
4939265	14	−3.077	−2.411	3.923	51.99	0.42	6.4
4990413	4	−3.029	−2.522	3.923	83.86	0.12	1.8
5008689	5	−3.123	−2.744	3.433	135.85	0.15	2.4
5015542	8	−2.952	−2.305	3.923	47.08	0.24	4.0
5016904	4	−2.854	−2.512	4.414	20.11	0.12	2.1
5079590	12	−2.869	−2.154	3.923	34.33	0.36	5.7
5131463	3	−2.949	−2.733	3.433	238.35	0.09	1.3
5167100	3	−3.087	−2.755	4.904	157.92	0.09	1.6
5182822	1	−2.331	−2.164	4.904	0.00	0.03	0.6
5217339	4	−3.081	−2.520	3.923	223.14	0.12	2.1
5268904	5	−2.998	−2.630	3.433	96.12	0.15	2.2
5288534	11	−2.852	−2.155	3.923	44.63	0.33	5.1
5360082	5	−2.413	−2.071	4.414	51.00	0.15	2.7
5371494	4	−3.351	−2.793	3.923	143.20	0.12	2.0
5397422	7	−3.170	−2.652	3.433	28.94	0.21	3.4
5428088	13	−2.779	−2.410	3.433	43.16	0.39	6.3
5437459	12	−2.942	−2.472	3.923	53.46	0.36	5.6
5461756	12	−3.242	−2.844	3.433	52.97	0.36	5.6
5513266	6	−2.402	−2.061	3.433	117.70	0.18	2.7
5516671	12	−2.567	−2.066	3.923	33.84	0.36	6.2
5607395	8	−2.747	−2.329	3.923	99.56	0.24	3.6
5648400	6	−3.159	−2.805	4.414	61.30	0.18	3.0

Table 2—Continued

Kepler ID	#	Log EW_{phot}	Log $\Delta F/F$	Median Duration (hours)	$t_{between}$ (hours)	ν (hours^{-1})	% flaring
5693747	1	−2.546	−2.265	5.395	0.00	0.03	0.7
5694127	8	−3.003	−2.383	3.433	51.00	0.24	3.8
5702236	3	−2.914	−2.701	3.433	25.99	0.09	1.2
5709193	5	−2.928	−2.475	3.923	50.02	0.15	2.4
5722668	5	−3.110	−2.743	3.923	79.94	0.15	2.5
5729898	7	−2.682	−2.316	3.923	110.84	0.21	3.6
5732553	3	−3.023	−2.500	3.923	7.36	0.09	1.6
5770769	5	−2.569	−2.050	4.904	42.67	0.15	3.1
5784256	7	−2.815	−2.226	3.923	77.98	0.21	3.6
5855096	2	−2.654	−2.241	5.395	359.97	0.06	1.0
5858361	9	−3.144	−2.778	4.414	49.04	0.27	4.5
5859365	6	−2.494	−2.298	4.904	88.28	0.18	3.5
5952853	5	−3.335	−3.113	3.433	14.71	0.15	2.4
5962532	12	−2.736	−2.418	3.923	43.65	0.36	5.9
5992270	2	−2.943	−2.647	4.414	401.66	0.06	1.0
6021431	3	−3.299	−2.793	3.433	364.88	0.09	1.4
6029338	2	−2.704	−2.256	4.904	402.64	0.06	1.1
6033083	3	−2.962	−2.503	3.923	260.42	0.09	1.4
6038882	1	−2.614	−2.278	5.395	0.00	0.03	0.7
6045059	6	−2.793	−2.605	3.923	57.38	0.18	2.9
6100469	1	−2.767	−2.321	4.414	0.00	0.03	0.5
6116129	6	−3.016	−2.816	4.414	46.59	0.18	3.4
6119605	3	−2.997	−2.606	4.414	78.47	0.09	1.6
6141300	3	−2.708	−2.370	4.414	189.80	0.09	1.6
6146804	3	−3.361	−2.870	3.923	50.02	0.09	1.3
6224062	14	−3.192	−2.775	3.433	43.65	0.42	6.0
6263016	10	−2.797	−2.415	3.923	50.02	0.30	4.6
6290789	10	−3.026	−2.644	3.433	47.08	0.30	4.3
6290811	11	−2.925	−2.402	3.923	44.63	0.33	5.2
6310265	9	−2.418	−2.098	3.923	85.82	0.27	4.5
6356144	4	−2.657	−2.486	4.414	25.99	0.12	2.3
6380533	2	−2.936	−2.539	4.414	16.18	0.06	0.9
6425928	4	−2.993	−2.391	3.433	198.62	0.12	2.0
6431497	6	−3.163	−2.786	3.923	25.50	0.18	3.0
6510289	7	−2.965	−2.531	3.433	56.89	0.21	3.2
6521729	3	−2.968	−2.630	2.943	60.81	0.09	1.3
6522124	4	−3.182	−2.631	3.923	43.16	0.12	1.8
6542087	7	−3.087	−2.608	3.433	61.79	0.21	3.1
6547641	4	−2.652	−2.282	4.904	137.32	0.12	2.1
6548898	5	−3.034	−2.577	4.414	101.52	0.15	2.6
6606167	7	−3.155	−2.628	3.923	60.32	0.21	3.6
6608436	5	−2.643	−2.478	3.433	54.93	0.15	2.5
6610837	5	−2.900	−2.575	3.433	68.66	0.15	2.3
6620003	9	−2.906	−2.456	3.923	53.95	0.27	4.5
6668646	10	−2.637	−2.351	3.923	34.33	0.30	4.8
6668936	1	−3.427	−2.924	3.923	0.00	0.03	0.5
6674908	12	−3.036	−2.777	3.433	54.44	0.36	5.7
6675714	11	−2.914	−2.578	3.923	46.59	0.33	5.4

Table 2—Continued

Kepler ID	#	Log EW_{phot}	Log $\Delta F/F$	Median Duration (hours)	$t_{between}$ (hours)	ν (hours^{-1})	% flaring
6763067	5	−2.659	−2.374	4.414	92.69	0.15	2.7
6766663	5	−3.237	−2.957	3.923	30.90	0.15	2.3
6767913	3	−3.028	−2.576	3.923	99.07	0.09	1.5
6783369	7	−3.102	−2.753	3.433	34.33	0.21	3.2
6843185	8	−2.146	−2.035	4.904	53.46	0.24	4.5
6846570	4	−2.581	−2.502	4.414	319.27	0.12	2.1
6863726	3	−3.280	−2.774	3.923	161.35	0.09	1.5
6871896	10	−3.047	−2.644	3.923	69.15	0.30	4.9
6928206	13	−3.219	−2.768	3.923	45.61	0.39	6.1
6949412	4	−2.305	−2.046	4.904	75.04	0.12	2.1
7017604	8	−3.006	−2.715	3.433	92.69	0.24	3.9
7018323	4	−2.891	−2.598	3.923	49.53	0.12	1.9
7031565	3	−3.212	−2.659	3.923	29.92	0.09	1.4
7107430	10	−3.399	−3.006	3.433	75.04	0.30	4.5
7133807	6	−2.528	−2.375	4.904	110.35	0.18	3.2
7188204	7	−2.666	−2.233	4.414	94.16	0.21	3.7
7191311	14	−2.844	−2.515	3.433	47.08	0.42	6.1
7192199	5	−2.944	−2.425	3.433	61.79	0.15	2.5
7215890	5	−3.460	−3.003	3.433	152.52	0.15	2.3
7218950	6	−2.396	−2.122	4.904	127.51	0.18	3.3
7281399	3	−3.101	−2.461	3.433	281.50	0.09	1.3
7293120	5	−3.080	−2.669	3.923	176.55	0.15	2.5
7347797	3	−3.083	−2.673	3.923	83.37	0.09	1.5
7347999	5	−3.379	−3.019	3.433	115.25	0.15	2.3
7381180	10	−2.882	−2.248	3.923	33.84	0.30	4.9
7422811	11	−2.669	−2.130	3.433	72.58	0.33	5.0
7456455	6	−3.229	−2.725	3.923	88.77	0.18	2.9
7461212	6	−2.795	−2.262	3.923	71.60	0.18	3.1
7465605	13	−3.249	−2.971	3.433	50.51	0.39	5.7
7509281	9	−2.667	−2.262	3.433	84.35	0.27	3.8
7509473	6	−3.302	−2.859	3.923	82.88	0.18	2.9
7509496	5	−3.018	−2.650	3.433	55.42	0.15	2.3
7551695	4	−1.814	−1.720	5.395	43.16	0.12	2.3
7592133	9	−2.677	−2.403	2.943	30.41	0.27	3.9
7670700	4	−2.988	−2.743	3.923	101.03	0.12	2.1
7677767	7	−3.566	−3.190	3.433	29.43	0.21	3.4
7692454	10	−3.210	−2.946	3.923	66.70	0.30	4.7
7751342	6	−2.905	−2.519	3.433	38.25	0.18	2.6
7772109	2	−3.426	−2.961	4.904	94.65	0.06	1.0
7830341	10	−2.811	−2.457	3.923	70.62	0.30	5.3
7830503	1	−2.273	−2.044	5.885	0.00	0.03	0.7
7836762	3	−3.739	−2.906	3.923	215.79	0.09	1.7
7849619	1	−1.544	−1.438	5.885	0.00	0.03	0.7
7871438	11	−2.696	−2.485	3.923	66.70	0.33	5.7
7877209	12	−2.750	−2.401	2.943	52.48	0.36	5.3
7885309	8	−2.768	−2.473	3.923	139.77	0.24	4.2
7907119	15	−3.113	−2.747	3.433	32.86	0.45	7.1
7936309	11	−2.801	−2.358	3.923	54.44	0.33	5.4

Table 2—Continued

Kepler ID	#	Log EW_{phot}	Log $\Delta F/F$	Median Duration (hours)	$t_{between}$ (hours)	ν (hours^{-1})	% flaring
7937049	5	−2.763	−2.372	3.433	147.62	0.15	2.3
7959162	1	−3.617	−2.966	3.923	0.00	0.03	0.5
7987934	3	−2.692	−2.340	3.923	49.53	0.09	1.5
8004647	4	−2.451	−2.210	4.414	184.89	0.12	2.3
8007234	7	−2.643	−2.238	3.923	50.51	0.21	3.3
8042251	4	−3.910	−3.479	3.923	102.50	0.12	2.0
8104467	4	−2.602	−2.351	4.414	60.32	0.12	2.0
8149782	3	−3.017	−2.459	3.923	110.84	0.09	1.4
8176468	11	−3.399	−2.854	3.433	15.69	0.33	5.3
8196449	14	−2.725	−2.474	3.433	43.16	0.42	6.5
8249046	2	−2.727	−2.423	4.904	322.70	0.06	1.0
8292758	8	−2.413	−1.872	3.433	74.55	0.24	3.8
8302555	7	−2.805	−2.333	3.433	83.37	0.21	3.1
8316096	9	−3.349	−2.822	3.433	59.83	0.27	4.0
8321490	7	−2.998	−2.569	3.433	74.54	0.21	3.2
8343785	5	−2.699	−2.259	3.433	58.85	0.15	2.3
8376893	8	−2.771	−2.343	4.414	80.43	0.24	3.8
8416925	2	−3.092	−2.568	4.904	476.69	0.06	1.0
8456954	5	−2.851	−2.477	3.923	78.47	0.15	2.3
8479655	7	−2.949	−2.616	4.414	59.83	0.21	3.8
8482565	6	−2.643	−2.502	4.414	155.96	0.18	3.2
8487242	12	−3.051	−2.437	3.923	49.53	0.36	5.7
8491152	8	−2.987	−2.669	2.943	70.13	0.24	3.3
8540644	3	−3.183	−2.917	2.943	85.82	0.09	1.5
8546579	6	−3.034	−2.808	3.923	93.18	0.18	3.1
8560255	1	−3.254	−2.983	3.433	0.00	0.03	0.4
8572338	8	−2.981	−2.488	3.433	24.52	0.24	3.7
8604575	3	−2.661	−1.925	3.923	216.28	0.09	1.6
8617530	3	−3.235	−2.733	4.414	157.43	0.09	1.5
8620472	2	−3.218	−2.412	3.923	71.60	0.06	1.0
8651471	6	−2.994	−2.651	4.904	136.83	0.18	3.6
8684857	1	−3.113	−2.554	3.433	0.00	0.03	0.4
8776565	7	−2.959	−2.605	3.433	55.91	0.21	3.2
8845205	2	−2.895	−2.458	4.414	129.47	0.06	1.0
8881943	7	−3.073	−2.387	3.923	87.30	0.21	3.3
8935140	6	−2.402	−2.194	4.414	102.01	0.18	3.2
8947255	11	−2.726	−2.347	3.433	47.57	0.33	5.1
8959288	11	−3.041	−2.662	3.433	58.36	0.33	5.0
9002074	6	−2.791	−2.338	3.923	62.28	0.18	3.1
9030716	5	−3.161	−2.744	3.433	32.86	0.15	2.3
9048551	8	−2.940	−2.659	4.414	26.48	0.24	3.8
9048949	8	−3.037	−2.503	4.414	96.12	0.24	4.3
9051905	2	−2.651	−2.300	5.395	635.10	0.06	1.2
9117167	2	−3.162	−2.692	4.904	288.37	0.06	1.1
9159012	9	−3.620	−3.051	3.433	54.93	0.27	4.0
9163591	5	−2.508	−2.310	4.414	38.25	0.15	2.7
9179906	10	−2.540	−2.132	3.923	58.85	0.30	4.8

Table 2—Continued

Kepler ID	#	Log EW_{phot}	Log $\Delta F/F$	Median Duration (hours)	$t_{between}$ (hours)	ν (hours^{-1})	% flaring
9180393	5	−2.938	−2.408	3.923	58.36	0.15	2.4
9214598	5	−3.144	−2.844	3.923	91.71	0.15	2.5
9220002	7	−2.676	−2.356	4.414	60.81	0.21	3.7
9224698	6	−3.041	−2.563	3.923	89.26	0.18	2.9
9238899	8	−2.707	−2.333	4.414	54.93	0.24	4.3
9239775	4	−3.181	−2.686	4.414	133.89	0.12	2.0
9267818	6	−2.632	−2.341	3.433	115.25	0.18	2.5
9269688	11	−3.257	−2.600	3.433	18.64	0.33	4.9
9346592	12	−2.948	−2.431	3.923	63.76	0.36	5.6
9349698	13	−2.631	−2.467	5.395	48.55	0.39	8.5
9395205	12	−2.841	−2.627	3.923	66.70	0.36	5.7
9407581	10	−2.578	−2.315	3.433	64.25	0.30	4.7
9425635	3	−3.146	−2.531	3.923	194.70	0.09	1.4
9428095	3	−2.631	−2.100	4.904	137.81	0.09	1.6
9450669	9	−2.130	−1.857	4.414	9.32	0.27	4.9
9468935	7	−3.166	−2.818	3.433	50.02	0.21	3.0
9474589	6	−3.392	−2.935	3.433	115.25	0.18	2.6
9480850	4	−3.124	−2.743	3.433	170.67	0.12	1.7
9508099	3	−2.526	−2.261	3.923	65.72	0.09	1.5
9530263	6	−3.091	−2.503	3.433	131.92	0.18	2.7
9540467	12	−3.209	−2.864	3.923	44.63	0.36	6.0
9570305	5	−2.909	−2.426	3.923	96.12	0.15	2.4
9576197	6	−2.775	−2.175	4.414	115.25	0.18	3.2
9579266	1	−2.576	−2.246	4.414	0.00	0.03	0.5
9581885	8	−2.827	−2.531	3.433	63.27	0.24	3.5
9588880	7	−2.826	−2.536	3.923	44.14	0.21	3.5
9596620	3	−2.975	−2.535	4.414	101.52	0.09	1.6
9613610	4	−2.925	−2.594	4.414	111.82	0.12	2.2
9631366	8	−2.966	−2.635	3.923	78.96	0.24	4.0
9637196	3	−3.368	−3.130	3.923	51.00	0.09	1.5
9659036	4	−2.899	−2.455	3.923	42.18	0.12	1.9
9697509	4	−3.077	−2.526	3.433	130.45	0.12	1.6
9713986	5	−2.676	−2.352	4.414	42.18	0.15	2.6
9765275	4	−3.012	−2.530	3.923	158.41	0.12	2.0
9784213	5	−2.611	−2.364	3.923	13.24	0.15	2.6
9838763	6	−2.536	−2.352	4.904	199.11	0.18	3.3
9880382	7	−2.849	−2.438	4.414	72.09	0.21	3.7
9892651	8	−2.446	−2.276	3.923	30.41	0.24	4.0
9909614	5	−3.298	−2.770	3.923	63.26	0.15	2.3
9941718	11	−2.535	−2.206	3.923	32.86	0.33	5.6
9945771	9	−2.442	−1.882	3.923	44.63	0.27	5.1
9969320	2	−2.786	−2.443	3.923	438.44	0.06	0.9
10002792	6	−3.046	−2.334	3.923	43.16	0.18	3.1
10011038	5	−2.760	−2.391	3.923	79.94	0.15	2.4
10056727	7	−2.843	−2.525	3.923	48.55	0.21	3.5
10065745	6	−2.472	−2.099	5.395	114.27	0.18	3.7
10070247	6	−1.965	−1.792	4.904	100.54	0.18	3.3
10134498	4	−2.616	−2.408	4.414	80.43	0.12	2.1

Table 2—Continued

Kepler ID	#	Log EW_{phot}	Log $\Delta F/F$	Median Duration (hours)	$t_{between}$ (hours)	ν (hours^{-1})	% flaring
10139305	4	−2.841	−2.470	4.904	68.17	0.12	2.4
10165244	8	−2.929	−2.244	3.923	57.38	0.24	4.0
10188460	8	−3.284	−2.838	4.414	76.02	0.24	4.0
10196750	7	−3.005	−2.494	3.433	75.04	0.21	3.3
10208370	6	−3.020	−2.547	3.923	170.18	0.18	2.9
10288161	6	−2.935	−2.493	4.414	60.81	0.18	3.3
10317398	4	−2.306	−2.027	5.395	216.28	0.12	2.5
10319112	6	−2.917	−2.440	3.923	53.95	0.18	3.1
10320656	9	−3.586	−3.060	3.433	73.56	0.27	4.1
10363074	8	−2.703	−2.348	3.923	61.79	0.24	4.0
10397709	6	−2.071	−1.584	5.395	31.39	0.18	3.5
10422252	12	−2.969	−2.688	4.414	52.48	0.36	6.2
10449542	3	−2.751	−2.345	3.923	72.09	0.09	1.5
10471960	6	−2.333	−2.083	4.904	61.30	0.18	3.2
10513641	4	−2.627	−2.279	3.923	72.09	0.12	1.8
10518758	5	−3.075	−2.493	3.923	128.00	0.15	2.2
10528093	5	−2.549	−2.326	5.395	56.40	0.15	3.1
10536761	6	−2.558	−2.197	4.414	135.85	0.18	3.1
10548015	2	−2.779	−2.324	5.395	381.55	0.06	1.1
10622511	9	−3.276	−2.900	3.923	60.32	0.27	4.4
10658494	10	−2.948	−2.573	3.923	55.91	0.30	5.1
10727657	5	−3.446	−2.942	3.923	110.35	0.15	2.4
10753072	7	−2.941	−2.502	3.923	44.14	0.21	3.4
10779266	5	−2.891	−2.548	3.923	142.71	0.15	2.4
10790838	5	−2.599	−2.261	4.414	77.00	0.15	2.7
10793290	2	−2.855	−2.304	3.923	104.95	0.06	0.9
10801273	6	−4.073	−3.644	3.923	44.14	0.18	2.7
10818065	9	−2.731	−2.377	3.923	38.74	0.27	4.8
10857583	5	−2.409	−2.085	5.395	65.72	0.15	3.2
10865206	6	−2.865	−2.229	3.923	152.52	0.18	3.2
10872868	9	−2.937	−2.565	3.923	97.59	0.27	4.7
10905040	3	−2.673	−2.400	4.904	183.91	0.09	1.9
10938188	5	−2.866	−2.561	3.433	32.37	0.15	2.4
10960823	11	−2.637	−2.283	3.923	39.72	0.33	5.3
10975238	8	−2.534	−2.138	4.414	45.61	0.24	4.3
10990728	1	−2.749	−2.444	4.904	0.00	0.03	0.6
10991547	5	−3.003	−2.387	3.923	136.83	0.15	2.3
11017875	9	−2.946	−2.453	3.923	51.49	0.27	4.2
11032573	7	−2.939	−2.435	3.923	87.30	0.21	3.6
11037498	4	−2.965	−2.638	3.923	103.48	0.12	2.0
11047115	8	−2.708	−2.477	4.414	44.63	0.24	4.1
11068661	4	−1.796	−1.646	5.395	20.60	0.12	2.2
11081377	6	−3.196	−2.888	3.923	118.19	0.18	2.9
11124203	12	−3.003	−2.312	3.923	29.43	0.36	5.6
11128748	2	−3.201	−2.744	4.904	104.95	0.06	1.0
11190713	9	−2.903	−2.398	3.433	31.39	0.27	4.2
11190969	6	−3.429	−2.955	3.433	107.89	0.18	2.9
11190988	4	−3.293	−2.891	4.414	191.76	0.12	2.0

Table 2—Continued

Kepler ID	#	Log EW_{phot}	Log $\Delta F/F$	Median Duration (hours)	$t_{between}$ (hours)	ν (hours^{-1})	% flaring
11192887	7	−2.967	−2.700	3.923	52.97	0.21	3.4
11196403	9	−2.893	−2.515	3.433	48.06	0.27	4.2
11244150	9	−2.747	−2.362	3.923	72.09	0.27	4.5
11251134	3	−2.520	−2.173	4.904	124.57	0.09	1.7
11342883	8	−2.753	−2.508	4.904	82.39	0.24	4.6
11465987	4	−2.671	−2.343	5.885	99.07	0.12	2.7
11493667	5	−3.013	−2.410	3.433	49.53	0.15	2.4
11515276	7	−2.436	−2.167	3.923	61.79	0.21	3.4
11521274	3	−3.084	−2.738	3.923	33.84	0.09	1.5
11550428	10	−2.856	−2.499	3.923	41.69	0.30	4.3
11569291	5	−2.899	−2.541	2.943	151.54	0.15	2.1
11612409	2	−3.384	−2.915	3.923	424.22	0.06	0.9
11658934	7	−3.096	−2.525	3.923	27.95	0.21	3.3
11662738	5	−2.335	−2.114	4.414	127.02	0.15	2.8
11663521	7	−3.737	−3.130	3.923	39.72	0.21	3.7
11717648	13	−3.053	−2.750	3.433	50.02	0.39	5.7
11721444	3	−3.056	−2.615	4.904	125.06	0.09	1.8
11808734	12	−2.732	−2.277	3.923	34.33	0.36	5.9
11824222	4	−3.082	−2.849	3.433	340.35	0.12	1.6
11859900	8	−2.947	−2.499	3.923	82.88	0.24	3.7
11870769	4	−1.932	−1.721	4.904	69.15	0.12	2.3
11873179	1	−2.135	−1.899	4.414	0.00	0.03	0.5
11958955	9	−3.136	−2.682	3.923	54.44	0.27	4.3
11969772	3	−3.016	−2.663	4.414	88.28	0.09	1.6
12004872	10	−2.787	−2.478	3.923	69.15	0.30	5.2
12061183	6	−2.969	−2.498	3.923	114.76	0.18	2.7
12105694	4	−2.656	−2.268	3.923	127.51	0.12	2.0
12117857	1	−2.424	−2.183	5.885	0.00	0.03	0.7
12254596	2	−3.271	−2.858	4.904	281.01	0.06	1.0
12258055	9	−2.854	−2.298	3.923	15.69	0.27	4.8
12303977	4	−1.526	−1.250	5.395	171.16	0.12	2.5
12314646	16	−2.869	−2.171	3.923	26.48	0.48	7.7
12356051	9	−2.749	−2.226	3.433	50.51	0.27	4.0
12401644	10	−2.796	−2.505	4.414	73.56	0.30	5.4
12599435	2	−2.843	−2.392	3.923	83.86	0.06	1.0
12599998	3	−2.873	−2.418	2.943	115.25	0.09	1.2
12735599	4	−2.922	−2.436	4.414	104.95	0.12	2.0
12835232	3	−2.971	−2.507	3.433	97.10	0.09	1.5